

NEAR—WALL CHARACTERISTICS OF TURBULENT FLOW BEHIND LATERALLY SPACED CIRCULAR CYLINDERS

*A Thesis Submitted
in Partial Fulfilment of the Requirements
for the degree of*
MASTER OF TECHNOLOGY

by
MASOOD SHARIEF

to the
**DEPARTMENT OF CIVIL ENGINEERING
INDIAN INSTITUTE OF TECHNOLOGY KANPUR**
NOVEMBER, 1989

V.90

- 4 APR 1990

CENTRAL LIBRARY
I. I. T., KANPUR

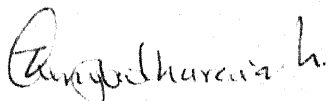
Acc. No. A107868

CE-1998-M-SHA-NEA


Th
532.54
Sh 23n

C E R T I F I C A T E

The thesis entitled, "Near - Wall Characteristics of Turbulent Flow Behind Laterally Spaced Circular Cylinders", by Masood Sharief (Roll No. 8720310) is hereby approved as a creditable report on research carried out and presented in a manner which warrants its acceptance as a prerequisite for the degree of Master of Technology. The work has been carried out under our supervision and has not been submitted elsewhere for award of a degree.



(DR. T. GANGADHARAIYAH)
PROFESSOR
DEPARTMENT OF CIVIL ENGG.
I.I.T. KANPUR.



(DR. A.K. GUPTA)
PROFESSOR AND HEAD
DEPARTMENT OF AERONAUTICAL
ENGG., I.I.T. KANPUR.

November, 1989.

ACKNOWLEDGEMENTS

The author lacks words to express his sincerest gratitude to Dr. T. Gangadharaiah and Dr. A.K. Gupta for their constant help, valuable guidance and encouragement during the work.

The author must also thank Dr. K. Subramanya, Dr. V. Lakshminarayana, Dr. S. Ramaseshan, Dr. S. Surya Rao Dr. B.S. Murthy of Department of Civil Engineering.

Whole hearted thanks to Mr. Muddappa, for his timely help and encouragement during the experiment.

Special thanks to Mr. Musammil and Mr. Gautam Roy, graduate students, for their kind help and suggestions throughout the work.

The cooperation received from the staff of Hydraulics Laboratory of the Department of Civil Engineering is gratefully acknowledged.

Thanks are due to my friends who were involved directly or indirectly in my work.

Finally, thanks to Mr. G.S. Trivedi and Mr. M.L. Bhatia for excellent typing and to Mr. A.K. Ganguli for drawings.

- MASOOD SHARIEF

CONTENTS

	<u>Page</u>
LIST OF FIGURES	v
NOTATIONS	vii
ABSTRACT	ix
CHAPTER 1 INTRODUCTION	1
CHAPTER 2 LITERATURE REVIEW	
2.1 Flow Characteristics at the Junction of Cylinder and Wall	3
2.2 Scouring Phenomenon Around Single Pier	4
2.3 Scouring Phenomenon Around Multiple Pier	5
2.4 Base Pressure Distribution and Velocity Profile	7
2.5 Interference Effects in the Free Stream Region	8
2.5.1 Tandem Arrangements	8
2.5.2 Side by Side Arrangement	9
2.5.3 Staggered Arrangement	11
2.6 Summary of Hydrodynamic Effects	11
2.6.1 Tandem Arrangement	11
2.6.2 Side by Side Arrangement	12
2.6.3 Staggered Arrangement	13
2.7 Present Investigation	13
CHAPTER 3 HOT FILM ANEMOMETRY AND CALIBRATION	
3.1 General	15
3.2 Anemometry	17
3.2.1 Constant Temperature Anemometer	17
3.2.2 Constant Current Anemometer	18
3.3 Calibration of the Probe	18
3.3.1 Heat Transfer Law for Sensor (King's Law)	19

	<u>Page</u>
CHAPTER 4 EXPERIMENTAL SET-UP, INSTRUMENTATION AND PROCEDURE	
4.1 Experimental Setup	21
4.2 Instrument Details	22
4.3 Experimental Procedure	26
CHAPTER 5 ANALYSIS OF RESULTS AND DISCUSSIONS	
5.1 Lateral Profiles of Mean Velocity and RMS Velocity Near the Wall	30
5.2 Vertical Profiles of Mean Velocity and RMS Velocity	40
5.3 Variation of RMS Velocity at the Edge of the Wake	45
5.4 Comparison of RMS Velocity Profiles at the Centre, Edge and Outside the Wake Region	45
5.5 Mean Velocity Distribution in the Vertical Direction	48
5.6 RMS Velocity Distribution in Vertical Direction	52
5.6.1 Behind the Cylinder ($Y=0$)	52
5.6.2 Between Cylinders ($Y = S/2$)	55
5.7 Mean Velocity Distribution in the Lateral Direction Near the Wall	57
5.8 Interference Effect of Cylinders	61
CHAPTER 6 CONCLUSIONS AND SUGGESTIONS	
Conclusions	64
Suggestions	66
REFERENCES	67

LIST OF FIGURES

<u>Fig. No.</u>	<u>Title</u>	<u>Page</u>
3.1	Calibration curve	20
4.1	Schematic view of the wind tunnel	23
4.2	Definition sketch showing cylinder locations and Co-ordinate axes	29
5.1	Mean and RMS velocity profiles in lateral direction at $Z/D = 0.04$ for $S/D = \infty$	31
5.2	Mean and RMS velocity profiles in lateral direction at $Z/D = 0.04$ for $S/D = 5$.	32
5.3	Mean and RMS velocity profiles in lateral direction at $Z/D = 0.04$ for $S/D = 7$.	33
5.4	Mean and RMS velocity profiles in lateral direction at $Z/D = 0.04$ for $S/D = 9$.	34
5.5	Mean and RMS velocity contours for $S/D = \infty$ at $Z/D = 0.04$	36
5.6	Mean and RMS velocity contours for $S/D = 5$ at $Z/D = 0.04$	37
5.7	Mean and RMS velocity contours for $S/D = 7$ at $Z/D = 0.04$	38
5.8	Mean and RMS velocity contours for $S/D = 9$ at $Z/D = 0.04$	39
5.9	Mean and RMS velocity distribution in vertical direction along the centre line behind the cylinder	41
5.10	Mean and RMS velocity distribution in vertical direction along the centre line in between the cylinders	42
5.11	Maximum RMS velocity and it's position in vertical direction at $Y = 0$	44
5.12	Maximum RMS velocity and it's position in vertical direction at $Y = S/2$	44

<u>Fig. No.</u>	<u>Title</u>	<u>Page</u>
5.13	Longitudinal variation of $\frac{\sqrt{U'^2}}{U_0} \times 100$, $\frac{\sqrt{U'^2}}{U_0} \times 100 \frac{Y'}{D}$ at $Z/D = 0.04$	46
5.14	Vertical profiles of RMS velocity in the centre, edge and outside the wake region	47
5.15	Normalised mean velocity distribution in vertical direction behind the cylinder	49
5.16	Normalised mean velocity distribution in vertical direction in between the cylinders	50
5.17	Variation of power law exponent 'n' for velocity profiles	51
5.18	Maximum mean velocity and it's position in vertical direction at $Y=0$	53
5.19	Maximum mean velocity and it's position in vertical direction at $Y=S/2$	53
5.20	Normalised RMS velocity distribution in vertical direction behind the cylinder	54
5.21	Normalised RMS velocity distribution in vertical direction in between the cylinders	56
5.22	Velocity defect in the wake zone near the wall	58
5.23	Velocity defect outside the wake zone the wall	59
5.24	Longitudinal variation of $\frac{\bar{U}_c}{U_0}$ and $\frac{\bar{U}_b}{U_0}$ at $Z/D = 0.04$	60
5.25	Longitudinal variation of $\frac{b}{D}$ and $\frac{\bar{U}_b - \bar{U}_c}{U_0}$ at $Z/D = 0.04$	60
5.26	Longitudinal variation of $\frac{\sqrt{U'^2}}{U_0} \times 100$ at $Z/D = 1.0$.	63
5.27	Longitudinal variation of $\frac{U}{U_0}$ at $Z/D = 1.0$	63

NOTATIONS

R_{ep}	Pier Reynolds number.
S	Lateral Spacing at C/C .
X	Longitudinal spacing from the downstream edge of the cylinder.
X_c	Longitudinal spacing from the centre of the cylinder.
Y	Lateral direction.
Z	Vertical direction.
Y'	Distance from centre of the cylinder in lateral direction at which maximum RMS velocity occurs.
b	Distance from centre of the cylinder in lateral direction at which maximum mean velocity occurs.
D	Diameter of the cylinder.
V_o	Free stream velocity.
\bar{U}	Mean Velocity
\bar{U}_e	Maximum mean velocity in vertical direction behind the centre of the cylinder.
\bar{U}_{se}	Maximum mean velocity in vertical direc. along the centre line of spacing.
$\sqrt{\bar{U}^2}$	RMS velocity.
$\sqrt{\bar{U}_{max}^2}$	Maximum RMS velocity in lateral direction.
$\sqrt{\bar{U}_m^2}$	Maximum RMS velocity in vertical direc. behind the centre of the cylinder.
$\sqrt{\bar{U}_{ms}^2}$	Maximum RMS velocity in vertical dir. along the centre line of spacing.
\bar{U}_c	Mean velocity behind centre of the cylinder at $\frac{Z}{D} = 0.04$.
\bar{U}_b	Maximum mean velocity in lateral direction at $\frac{Z}{D} = 0.04$.
\bar{U}_{sc}	Mean velocity along the centre line of spacing at $\frac{Z}{D} = 0.04$.

- B Distance from centre line of spacing to the maximum mean velocity at $\frac{z}{D} = 0.04$.
- z_e Position of Maximum mean velocity in vertical direction behind the cylinder.
- z_{se} Position of Maximum mean velocity in along the centre line of spacing.
- z'_e Position of maximum RMS velocity in vertical direction behind the cylinder.
- z'_{se} Position of maximum RMS velocity in ^{direction} along the centre line of spacing.

ABSTRACT

The near - wall characteristics of turbulent boundary layer flow behind circular cylinders have been experimentally studied in this work. Two cylinders laterally separated at spacing(s) 5, 7, 9 and ∞ relative to cylinder diameter (D) were placed in a low - speed wind tunnel. The Mean and RMS fluctuating components of stream-wise velocity were measured near the wall on the leeside of cylinders upto distance 5D using hot film anemometer. Results indicate that the wake zone behind cylinders is of nearly uniform width, but increases slightly for $S = 9D$. The wall effect increases in the wake flow downstream of the cylinder where turbulence intensity is high. It is particularly high near the wake edges. In the central region between wakes the turbulence intensity appears relatively unaffected by the cylinders. However Mean flow is found to be accelerating, and velocities are higher than upstream undisturbed free-stream velocity. The flow is found to be accelerating, as evident also from the power law curves fitted to the vertical Mean velocity profiles. Interference effect of the two cylinders is evident in the Mean and RMS velocity distributions for $S = 5D$.

CHAPTER 1

INTRODUCTION

Rapid urbanisation and development of road transport and communication have necessitated construction of more and more bridges across rivers and waterways. The location of bridge piers in close proximity may involve interference effects of flow which results in scour depths different from that of isolated piers. While numerous investigations on scour depths have been made on the flow past a single pier having diverse shapes and flow conditions, very little attention has been focussed on lateral and longitudinal interference of bridge piers. Considerable research has been done when an obstruction is placed in the direction of flow. But such research was confined to the effects of free stream region which is of importance to Aeronautical engineers (twin struts to support the wings) and structural engineers (chimney stacks, offshore structures). Attention was not paid to what happens near the floor on which the obstruction is placed.

Hydraulic engineers are more concerned about this region because of scour and sediment problems associated with interference effects. Studies have been conducted in the hydraulics engineering laboratory, IIT Kanpur and elsewhere to determine the scour, flow characteristics near pier models when they are in tandem and staggered arrangements. However they are not exhaustive. In order to understand the effect of interference of piers on the scour depth, there was a need to study the effect of interference of flow in the wall region of the rigid bed. With this in view the

present work has been undertaken to study the wake characteristics of a single pier from the wall upto free stream and also to study the effect of interference of another cylinder placed by its side at different spacings.

The thesis is presented in six chapters. Chapter 1 introduces the problem and the scope of the present work. The relevant literature on the subject is described in Chapter 2, Hot Film Anemometry and it's calibration in Chapter 3, experimental setup, Instrumentation and procedure is explained in Chapter 4. Analysis of results and discussions are presented in Chapter 5. The thesis is concluded in Chapter 6 with suggestions for future work.

CHAPTER 2

LITERATURE REVIEW

Two cylinders in fluid flow act as isolated cylinders only when they are sufficiently apart. At close proximity the interference between the cylinders changes significantly the flow around them and produces unexpected forces and pressure distributions and intensifies or suppresses vortex characteristics. Hence, the flow around two circular cylinders may be classified into two categories: with and without interference. The interference may be either partial when only one cylinder is affected or combined when both mutually interfere.

2.1 FLOW CHARACTERISTICS AT THE JUNCTION OF CYLINDER AND WALL

The vortex filaments transverse to the flow in a two dimensional undisturbed velocity field are concentrated by the presence of a blunt-nosed pier. The concentration is accomplished by the non-uniform pressure field induced by the pier boundary. If the pressure field is sufficiently strong, a three dimensional separation of the boundary layer occurs which inturn, rolls up ahead of the pier to form the horse shoe vortex system.

The wake vortex system is formed by the rolling up of unstable shear layers generated by the surface of the cylinder and which are detached from either side of the cylinder at the separation line. At low cylinder Reynolds number ($4 < R_{ep} < 50$), these vortices are stable and form a standing system downstream close to the cylinder. For higher Reynold's numbers of practical

practical interest, the system is unstable and the vortices are shed alternately from the pier and convected downstream. The strength of the vortices in the wake system varies greatly according to the pier shape and fluid velocity.

The trailing vortex system is formed when finite pressure differences exist between two surfaces meeting at a corner such as the top of the pier. It is composed of one or more discrete vortices attached to the top of the pier and extending downstream. It usually occurs in the case of completely submerged piers.

Roper et. al. (1967) described in detail that the eddy structure may be composed of horse-shoe vortex system, the trailing vortex system and the wake vortex system depending upon the type of pier and free stream conditions. The vortex systems are an integral part of flow and strongly affect the vertical component of the velocity ahead of the pier.

2.2 SCOURING PHENOMENON AROUND SINGLE PIER

The basic cause of local scour is the hydrodynamic flow structure in the form of Horse shoe vortex which develops at the leading edge of the pier's junction with the bed. Shen, Schneider and Karaki classified the types of local scour based on the flow speed and emphasised the importance of pier geometry and pier Reynolds number. Similarity parameters characterising the horse shoe vortex flows were investigated experimentally by Belik (1973) in a low speed wind tunnel with the approaching boundary layers both laminar and turbulent. Baker (1979,1980) made extensive measurements of the static pressure

in the separated region of laminar and turbulent horse shoe vortices and showed the importance of Reynolds number for laminar horse shoe vortex using a fixed bed model of local scour zone, Melville and Raudkivi (1977) measured the turbulent intensities and the boundary shear stresses. Attempts have been made to estimate the vortex strength, core diameter and vortex centre locations of the primary horse shoe vortex by Baker (1979, 1980). Shen, Schneider and Karaki (1969), Baker (1980b), Qadar (1981), Gangadharaiah, Muzzammil and Subramanya (1986) have attempted to estimate the strength of horse shoe vortex and relate them to local scour.

2.3 SCOURING PHENOMENA AROUND MULTIPLE PIERS

There is considerable influence of location of the piers on scour depth as observed by various investigators like Dietz (1973), Basak et.al. (1975) and Elliot and Baker (1985). Dietz conducted tests with laterally separated circular piers and reported that, the maximum scour depth is not influenced by the angle of attack for centre line spacings S/D larger than 3.

Basak et.al. showed that for a row of square piers aligned with the flow, maximum scour always occurred at the upstream face of a pier with no influence of spacing and number of piers on scour depth. For other piers, minimum scour was observed for a centre line spacing $S/D = 4$. For spacings perpendicular to the flow, scour depth decreases with increasing spacing upto $S/D = 5$.

Elliot et.al. (1985) investigated the effect of lateral spacing on scour depth for clear water scour conditions. They found that as lateral spacing S/D , decreases, the scouring is affected by two processes:

- (i) The horse shoe vortices around the bases of the piers interact with each other
- (ii) The flow is accelerated by contraction of the flow region due to the piers.

This accelerated flow between the piers causes an increase in scour depth as lateral spacing S/D becomes small. If S/D is large, the depth of scour will not be affected by pier spacing. They pointed out that a careful study of interference effect of lateral spacing on scour depth for live bed scour conditions is further required.

Shah (1988) observed that the scour depth of a downstream pier in the tandem arrangement is less than that of isolated pier. He has compared the scour depths of the down stream pier in staggered arrangement for $\frac{S}{D} = 5, 7$ and 9 with the isolated pier scour depth. It was observed that in all the cases, except for $\frac{S}{D} = 5$, the down stream pier scour depth is greater than the isolated pier scour depth. The scour depth gradually increases to a maximum at $\frac{X}{D} = 6$ and decreases until $\frac{X}{D} = 10$. Then it gradually increases again and becomes constant for increasing $\frac{X}{D}$. He also observed in both the arrangement of piers for ripple bed flow condition that the scour depth at downstream pier is higher at $\frac{X}{D} = 1$ than when $\frac{X}{D} = 2$. He also concluded that as the lateral

spacing increases, the interference effect decreases. Hence for large $\frac{S}{D}$, scour depth approaches that of isolated pier's scour depth.

2.4 BASE PRESSURE DISTRIBUTION AND VELOCITY PROFILE

Hori (1959) showed that when two cylinders are in tandem arrangement, pressure distribution of only the rear part of upstream cylinder was affected by the presence of the downstream cylinder. The base pressure coefficient increased with spacing and consequently the drag of the upstream cylinder was reduced. This causes the decrease of the interference drag with corresponding increase of pressure in the gap only as observed by Bearman et.al. (1973), Bierman et.al.(1933), Shiraishi et.al.(1986). Thus, at critical spacing there is discontinuous decrease of the base pressure coefficient. Further increase of spacing brought little change in the base pressure coefficient.

Shiraishi et.al. (1986) concluded that $\frac{X_c}{D} = 5.5$ demarcates between positive and negative gap pressures corresponding to the spatial location of downstream cylinder inside or outside the wake of the upstream cylinder respectively. The steady pressure distribution of the downstream cylinder is located at the wake centreline of cylinders with $\frac{X_c}{D} = 3$. The position of reattachment points of the flow separated from the upstream cylinder was symmetrical and distance between them reduced as $\frac{X}{D}$ increased from 2 to 3.

Zdrakovich and Stanhope (1972) and Shiraishi et.al.(1986) showed that low velocity existed in the gap for all spacings upto 3.5. With further increase in the spacing there was a sudden

change of flow pattern in the gap.

Hori (1959) observed that there is a discontinuous change of base pressure coefficient for a transverse arrangement when $1.2 < S/D < 2.0$.

2.5 INTERFERENCE EFFECTS IN THE FREE STREAM REGION

2.5.1 Tandem Arrangements:

The following effects were observed by Biermann et.al. (1933), El-Taher (1985) and Hori (1959).

(i) Effects on Drag coefficient, C_D :

Drag coefficient of the downstream cylinder is strongly dependent on the pier Reynolds number, R_{ep} and longitudinal spacing, $\frac{X}{D}$. For all R_{ep} , the drag force on single cylinder is reached soon beyond the critical spacing $\frac{X}{D} \geq 4$, which means that the downstream cylinder has no effect on the upstream one.

Bearman and Wadcock (1973) observed instability in the flow when the gap between the cylinders is small ($0.1 \leq \frac{X_c}{D} < 1.0$) at $R_{ep} = 2.5 \times 10^4$. For $\frac{X_c}{D} > 4.0$, the interference drag could be positive or negative depending upon both R_{ep} and $\frac{X_c}{D}$. However, the interference drag on downstream cylinder for the tandem position was always negative for $\frac{X_c}{D} < 3$. Hence, the downstream cylinder experienced a forward thrust.

(ii) Vortex Shedding:

Haneen Kamp et.al. (1981) and Zdravovich (1977) found that a vortex street always forms behind the downstream cylinder, and also behind upstream cylinder when $\frac{X_c}{D} > 4$. The Strouhal number, S_t , decreased continuously with increasing spacing $1.0 \leq \frac{X_c}{D} \leq 4.0$.

A sudden jump occurred at $\frac{X_c}{D} \simeq 4$ for which vortex shedding was first detected behind the upstream cylinder.

According to Et-Taher (1985),

- (1) There is an abrupt change in the flow pattern for $\frac{X_c}{D} = 3.5$ accompanied by an abrupt change in pressure distribution and vortex shedding along the span of each cylinder.
- (2) For $\frac{X_c}{D} < 3.5$, there is no vortex shedding from the upstream cylinder. The vorticity shedding from downstream cylinder breaks down into a number of spanwise cells, the frequency being constant in each cell.
- (3) For $\frac{X_c}{D} > 3.5$, vortices are shed from both the cylinders such that the Strouhal number is constant along the span.

(iii) Surface Roughness Effects:

Surface roughness can promote transition to turbulence in the boundary layers around the circular cylinder and reduce the actual Reynolds number at which fully turbulent separation occurs.

2.5.2 Side by Side Arrangement:

- (i) Effects on Drag coefficient, vortex shedding and base pressure distributions:

Biermann and Hernstein (1933) showed that the interference drag was zero for all lateral spacings $\frac{S}{D} > 5$. The interference drag increased as the spacing decreased. For small spacings, very odd changes occurred. They remarked "Apparently the type of flow changes rapidly with a change in spacing. It may even change while the spacing is held constant." This was the first indication

of the bistable nature of two different flow patterns at these spacings.

Spivak (1946) measured the vortex shedding frequency behind two cylinders in the side-by-side arrangement. He found that for all transverse spacings $S/D > 2$ a single frequency in both wakes, reduced to Strouhal number, was the same as for the single cylinder. For $S/D < 2$, two different frequencies were recorded in both wakes. The upper frequency disappeared for small spacings and only the lower one continued down to the cylinders in contact.

Hori (1959) observed that there is a discontinuous change of the base pressure coefficient for a transverse arrangement when $1.0 < S/D < 2.0$. He also indicated that the wakes behind the cylinders were different from that of the single cylinder.

(ii) Bistable nature of Biased flow pattern:

It was observed that the vortex formation and shedding is markedly symmetric about the axis of the gap. At $S/D = 2.0$, the vortex shedding is still coupled, but the gap flow is slightly deflected upwards. The vortex shedding becomes uncoupled and weak $S/D = 1.5$, while the gap flow is biased to one side. The biased flow in the gap is bistable and intermittently changes over either downwards or upwards. Bearman et.al. (1973) discovered that the base pressure on both the cylinders fluctuate between the two extremes, in the range of spacings $1.0 \leq S/D \leq 2.3$. Thus, the bistable nature of the biased flow pattern was confirmed.

(iii) Lift and Drag Forces on two cylinders:

Due to the bistable nature of the flow the gap flow biased towards one cylinder will produce a resultant force on each

cylinder that is deflected relative to the free stream direction. The sum of the bistable high and low drag is always less than twice the drag of the single cylinder.

2.5.3 Staggered Arrangement :

Hori (1959) found the resultant interference force coefficient which is proportional to the drag coefficient vectors.

(i) Forces on the downstream cylinder:

It was observed that C_D increases regularly and gradually with S/D . The pressure distribution around the downstream cylinder indicated a bistable nature of the fully developed flow through the gap between the cylinders and no flow pattern similar to that found in the tandem arrangements at different spacing. Severe vibrations may be excited by the bistable gap flow (Zdravovich, 1977).

(ii) Effect of Reynolds Number:

It was observed that the wake behind a single cylinder narrows compared with the subcritical regime which causes a similar contraction of the interference boundary in the case of staggered arrangement (Zdravovich, 1977). A discontinuous suppression of the gap flow exists in the fully turbulent regime. The discontinuous jump in lift coefficient due to the gap flow is greater for the higher Reynolds number and the lower Reynolds number.

2.6 SUMMARY OF HYDRODYNAMIC EFFECTS

2.6.1 Tandem Arrangement:

Studies by El-Taher (1985), Shivaishi et.al. (1986), Shah (1988) indicate the following salient features:

- (1) The base pressure coefficient increased with spacing till a critical spacing is reached at ^{which it} decreased discontinuously. Further increase of spacing has little effect on the base pressure coefficient.
- (2) Low velocity existed in the gap for spacings upto 3.5. With further increase in the spacing there was sudden change of flow pattern in the gap.
- (3) The drag force and scour depths of downstream pier is less than that of isolated pier.
- (4) For all R_{ep} , the drag force on single cylinder is reached beyond critical spacing $\frac{X_c}{D} \geq 4$.
- (5) Vortex shedding always occurs behind downstream cylinder but for upstream cylinder only when $\frac{X_c}{D} > 4$.

2.6.2 Side by Side Arrangement:

Studies by Bienmann et.al. (1933), Spivak (1946), Hori (1959), Bearman et.al. (1973) indicate the following salient features:

- (1) The interference drag decreases with the spacing upto $\frac{S}{D} = \frac{4}{3}$, increases to a maximum around $\frac{S}{D} = 2.0$ and decreases with a further increase in $\frac{S}{D}$ value.
- (2) The base pressure decreases with increase in $\frac{S}{D}$ upto $\frac{4}{3}$, then increases with S/D , reaching a maximum value at $S/D = 2.0$ and remains fairly constant with further increase in S/D .
- (3) The drag force variation is similar to that of the base pressure.

- (4) The lift coefficient decreases rapidly as S/D is increased upto a value of about $4/3$ and for further spacings it remains essentially zero.

2.6.3 Staggered Arrangement:

Studies by Hori (1959) , Makovich (1977), Shah (1988) indicate the following salient features.

- (1) C_D increases regularly and gradually with S/D .
- (2) The pressure distribution around the downstream cylinder indicates a bistable nature of fully developed flow.
- (3) The discontinuous jump in the lift coefficient is greater for higher Reynolds number than for lower Reynolds number.
- (4) In all the cases studied by Shah (1988) ($S_D=5, 7$ and 9) except for $S/D = 5$, the downstream pier scour depth is greater than the isolated pier scour depth.

2.7 PRESENT INVESTIGATION

The aim of the present study is to understand the interference effect on scour depths, which necessitates a systematic study of interference effect on the rigid bed. In order to achieve this, the present work has been carried out in two phases. In the first phase, a single circular cylinder is used and the mean velocity and RMS velocity components have been studied behind the cylinder at different locations, ($X/D = 0.5, 1.0, 2.0, 3.0$ and 5.0) in a wind tunnel.

In the second phase, two circular cylinders are kept side by side at three different spacings ($S/D = 5.0, 7.0$ and 9.0) and the mean and RMS velocities have been studied behind the cylinders in a similar way to that of a single cylinder. Finally the results analysed and conclusions are given.

CHAPTER 3

HOT FILM ANEMOMETRY AND CALIBRATION

3.1 GENERAL

Almost all research in aerodynamics related to turbulence necessitates the measurement of components of mean velocity and fluctuating velocity. These can be measured suitably by using anemometers, namely:

- (i) Hot wire anemometer
- (ii) Hot film anemometer
- (iii) Laser Doppler Anemometer.

(i) Hot-wire Anemometer:

The hot-wire anemometer is widely used throughout the world in research laboratories. This is suitable for mean and fluctuating velocity measurements in air. Using this, measurements can also be made in liquids in other gases. In addition, the hot-wire anemometer can be used to determine the direction and speed of a fluid, to make turbulence measurements, to make measurements in compressible flows and to measure fluid temperature.

The hot wire probe is placed in the wind tunnel perpendicular to the flow direction where the velocity is to be measured. The wire becomes hot as current is passed through it, and the heat generated is dissipated mainly by convection. The heat loss by convection is dependent on parameters like velocity, temperature and the pressure of the medium where heat is dissipated. The resistance of the wire changes with a change in its temperature. Thus the voltage drop along the wire is related to the velocity of flow.

Hot wire anemometer has excellent frequency response; an upper frequency limit of 400 KHz is common for commercially available instruments. In addition it has excellent sensitivity at low velocity, good spatial resolution and an output signal in the form of a voltage difference for convenient data analysis.

The limitation of the hot wire anemometer is that it cannot be used in liquids and in some gases, which are highly contaminated. The ^{Probe} loses its sensitivity gradually. Even ordinary air dust damages the sensor due to impact by the dust particles. To overcome this problem Hot film anemometer was introduced.

(ii) Hot-Film Anemometer:

Due to the limitation of the hot wire anemometer ^{to} dust free air only, the more sophisticated, more general, rugged hot film anemometer was introduced with the aim to carry out research work in dense fluids, particularly in water. The sensor of a hot film probe is usually made of nickel or platinum deposited in a thin layer on a backing material, such as quartz and connected to the electronics package by leads attached to the ends of the film. A thin protective coating of quartz or other material is usually deposited over the film to prevent damage by abrasion or chemical reaction. There are different types of hot film probes available. Of these, wedge hot film probe and conical hot film probe are more popular. Conical type probe has been used in the present work. The working principle of the hot film anemometer is almost similar to that of the hot wire.

3.2 ANEMOMETRY

Three types of electronic packages are used, each controlling the sensor heating current in a different way. The most common is the constant temperature anemometer, which supplies a sensor heating current that varies with the fluid velocity, to maintain constant sensor resistance and thus constant sensor temperature. The second type is the constant current anemometer, which supplies a constant heating current to the sensor. The third type is the pulsed wire anemometer, which measures velocity by momentarily heating a wire to heat the fluid around it. This spot of heated fluid is convected downstream to a second wire that acts as a temperature sensor. The time of flight of the hot spot is inversely proportional to the fluid velocity.

3.2.1 Constant Temperature Anemometer:

The constant temperature anemometer system is simple to operate and can measure large velocity fluctuations. The idea behind the constant temperature system is to minimise the effect of probe thermal inertia by keeping the sensitive element at constant temperature and using the heating current as a measure of heat transfer and hence, also of velocity. Due to the very high gain, in the amplifier and the small mass of the sensor, the system is capable of responding to very rapid fluctuations in velocity.

The major advantage of constant temperature anemometer is that, its frequency response is high when compared with the frequency response of an un compensated constant current anemometer.

In the present work a constant temperature hot film anemometer is used.

3.2.2 Constant Current Anemometer:

In this mode, a constant current flows through the probe, independent of any resistance changes in the bridge. The probe resistance changes as a result of flow changes acting on the probe. The consequent voltage difference across the horizontal bridge diagonal is a measure of the flow velocity. As compared to the constant temperature anemometer, this mode is far less important in flow measurements. The hot film probes are hardly applicable at high frequencies when operated in the constant current mode as their frequency response cannot easily be compensated electronically. Still, the constant current anemometer principle is widely used for the measurement of temperature in which case the voltage difference across the bridge diagonal will then be a measure of the existing temperature.

3.3 CALIBRATION OF THE PROBE

The arduous part in hot film anemometry, is the proper interpretation of the voltage signal, calibration performs the job of co-relating the voltage with velocity. The hot film anemometer is a thermal device which relates the heat transfer from the heated probe to the flow velocity passing over it. It is therefore not an absolute measuring system and requires calibration. For calibration, a pitot tube is used to measure the actual velocity and relate it to the anemometer output voltage. In the present work, we have calibrated the probe in the actual wind tunnel in which

tests were conducted later. The pitot tube connected to a digital manometer is used to measure the flow velocity. A sufficient number of readings were taken at different dial settings of the meter of the windtunnel. On plotting the points thus obtained, it was found that they were along a straight line, as shown in Fig.3.1.

3.3.1 Heat Transfer Law for Sensor (King's Law):

A variety of heat transfer laws for heated sensors have been put forward. Of these, King's law is the most well known in hot wire anemometry, which describes the heat transfer from a cylinder of infinite length. It can be written as:

$$E_D^2 = A + B U^n$$

where E_D is the anemometer output voltage taken across the wheat stone bridge in the electronics package, U is the fluid velocity, A and B are constants. This equation although has certain limitations, is adequate for laboratory measurements at moderate velocities. The magnitude of the exponent ' n ' is found to be 0.5.

The sensor operating temperature is very important because it influences both the life of the probe and its sensitivity to velocity and ambient temperature changes. The sensor temperature is usually expressed as a ratio, called the over heat ratio, a , which is defined as

$$a = \frac{R_s}{R_f} \quad \text{or} \quad a = \frac{R_s - R_f}{R_f}$$

where R_s is the resistance of the heated sensor at its operating temperature, R_f is the resistance of the sensor at the temperature of the ambient fluid.

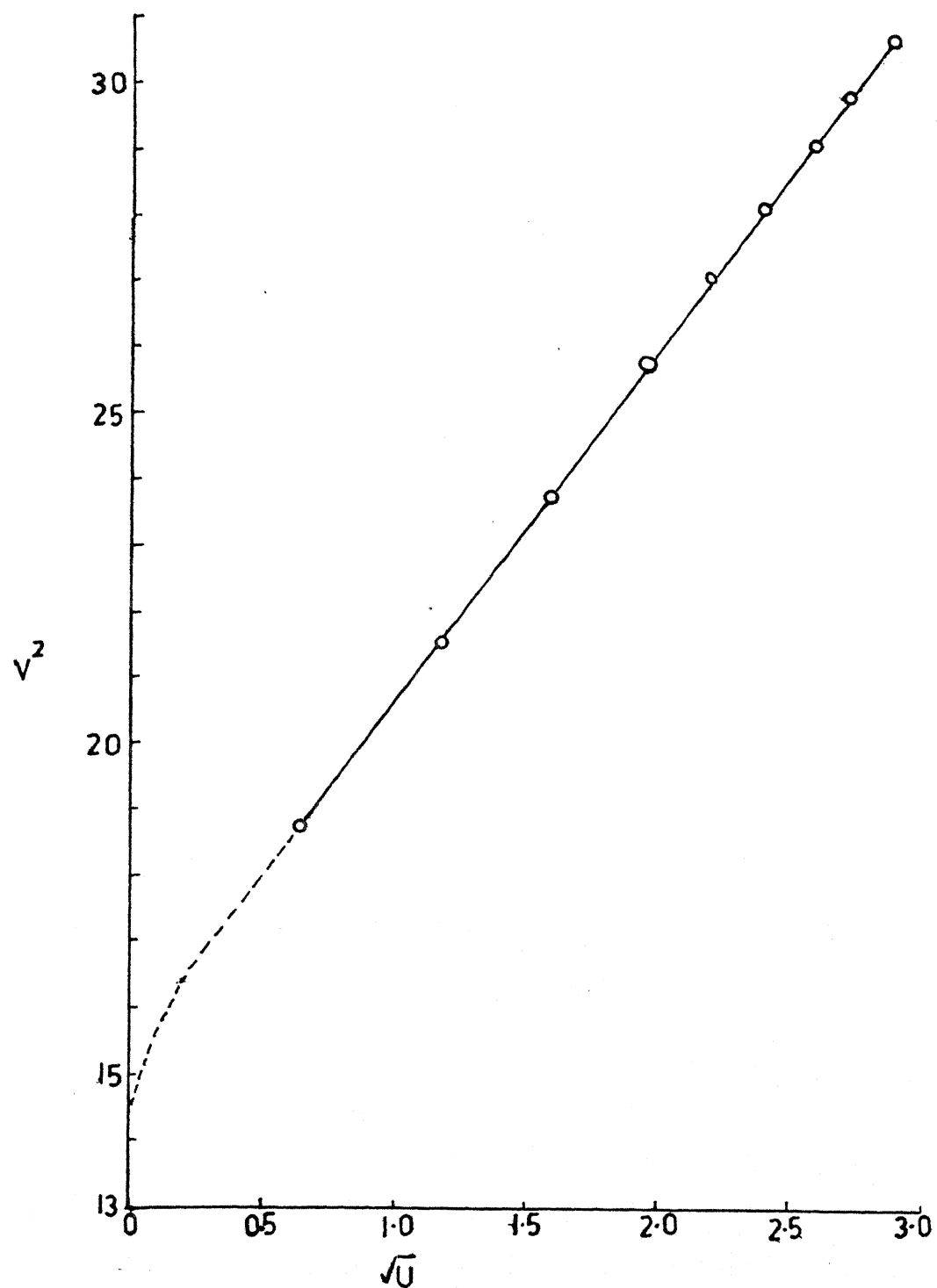


FIG 3-1 CALIBRATION CURVE

CHAPTER 4

EXPERIMENTAL SET UP, INSTRUMENTATION AND PROCEDURE

4.1 EXPERIMENTAL SETUP :

A wind tunnel is employed to simulate air streams under controlled laboratory conditions. The use of a wind tunnel gives an idea of fluid flow past a stationary object and evolution of certain flow patterns. The purpose of design of any wind tunnel is to achieve the required conditions for model and flow testing with minimum power consumption and at the smallest possible cost.

The present work has been carried out in a low speed, low turbulence, suction type, closed jet, open circuit wind tunnel of the Aerodynamics laboratory. The size of the test section of the wind tunnel is 30.5 cm height x 40.5 cm width x 101.6 cm long. The maximum speed in the clear test section is about 10 m/sec.

The tunnel has a settling chamber 2.5 cm square, with metal honey comb at it's entrance. There are six wire mesh screens located at appropriate intervals. An air filter made of cloth is also stretched across the tunnel inlet before the honey comb to minimise the entry of dust into the test section. The diffuser section following the test section is circular in cross-section and is achieved by the gradual divergence of the rectangular test section. At the end of the diffuser an

axial flow fan coupled to a 2 HP ducted DC variable speed motor having stabilised power supply provides a maximum wind speed of about 10 m/sec with a turbulence intensity of about 0.5%. A schematic view of the tunnel drawn to scale is shown in the Fig. 4.1.

THE TEST SECTION :

The top of the rectangular test section measuring 40.5 cm x 101.6 cm is covered with a 12 mm thick perspex sheet. It has a central longitudinal slot of width 22 cm x 50 cm. Special T plugs of appropriate size were fitted into the slot to prevent any leakage of air. The far side of the test section measuring 30.5 cm x 101.6 cm is a 6mm thick aluminium plate painted matt black. The bottom plate is made of a 6 mm thick perspex sheet. The front of the test section is made of a glass door hinged at the topedge, spanning the entire length of the test section.

4.2 INSTRUMENT DETAILS :

A DISA constant temperature anemometer (CTA), with a hot film probe has been used in the present work. The CTA consists of a main unit, a RMS voltmeter and a digital voltmeter.

The main unit 55 MD1 used in this work contains amplifier, filter, decade resistance, protection circuits

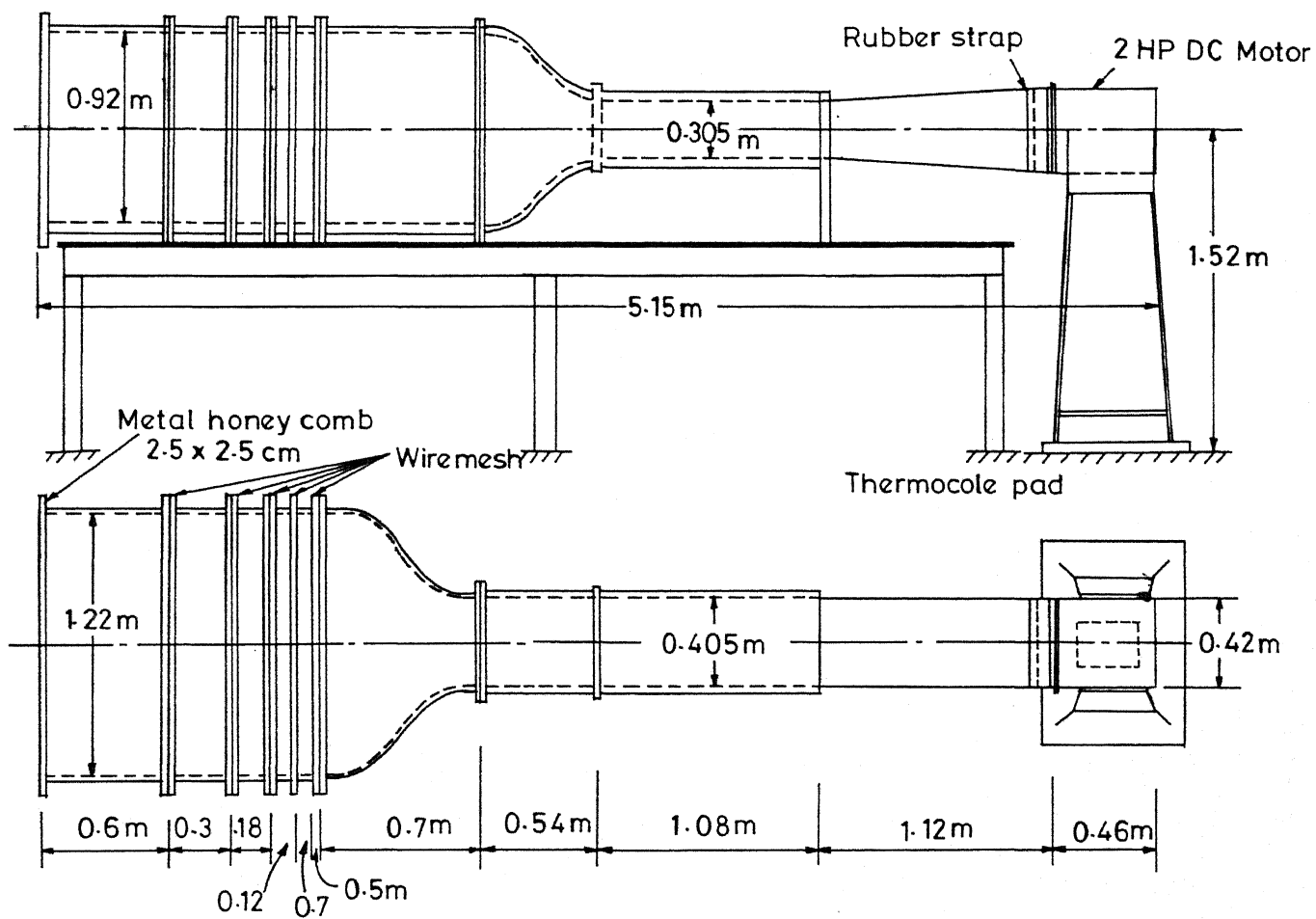


FIG 4-1 30.5 x 40.5 cm LOW SPEED LOW TURBULENCE WIND TUNNEL

and other auxiliary circuits. Meter sensitivity is switchable between 30V, 10V, 3V and 1V f.s.d. A 55 MD5 power pack is bolted to the main unit from behind in such a way that it constitutes an extension of the latter. A 55 M10 CTA standard bridge is also fixed to the main unit. It operates at a bridge ratio of 1:20. This facilitates connection of the input from the probe and output to the digital and RMS voltmeter.

A 55 D35 RMS voltmeter is used for measuring the RMS value of an AC voltage. This is a measure of the turbulence content of the flow under investigation. It has 12 ranges between 1mV to 300V and operates over the frequency range from 0.1 Hz to 400 kHz. Six different integrating time constants between 0.3 sec and 100 sec are available. For a given measurement, the integration time is increased till a steady value is displayed by the voltmeter. For most readings a 10 sec setting has been found to be adequate.

A 55 D31 Digital voltmeter used in this work has a max. error of 0.1% of full scale. This is used mainly for plotting calibration curves and for mean flow velocity measurements. This has a voltage range of 1.00, 10.00 and 100. It also has six different time constants between 0.3 and 100 secs. The degree of turbulence measured in the 55 D35 RMS voltmeter is digitalized here. It gives outstanding readability and high accuracy.

A Datametrics Type 1018 Electronic Manometer with digital read out was employed. For measurements of wind speeds, 25.4 mm of H_2O range was selected with a least count of 0.0001.

A conical hot film probe Type 55 R42 is used here. The details of the probe are :

Sensor resistance at $20^{\circ}C$, $R_{20} = 8.23$

Leads resistance, $R_L = 0.14$

Sensor TCR $\alpha_{20} = 0.042 \% / ^{\circ}C$

The probe was fixed to a long stainless steel tube of 4 mm internal diameter to facilitate mounting and traversing during the experiment. The sensor was inclined at an angle to the mean velocity vector which will reduce the likelihood of the probe fouling.

Polished circular brass cylinders of 25.4 mm diameter and 254 mm height were used in this experiment.

The Traversing Mechanism having three translational degrees of freedom is used for traversing the hot film probe. Two mechanical counters with provision for digital display were fitted to read the displacements. The resolutions in X (longitudinal), Y (lateral) and Z (vertical) directions were 0.125 mm, 0.05 mm and 0.05 mm respectively. To minimize the backlash in

the traverses, displacements in the X, Y and Z directions were increased or decreased monotonically.

4.3 EXPERIMENTAL PROCEDURE :

In the beginning, data was collected in the wind tunnel without any obstruction placed upstream. The hot film probe was traversed along the Z direction at the centre of the test section. Experiments show that there is no significant variation of flow quantities in the vertical direction above boundary layer. Hence, this data has not been reported here.

The present work has been carried out in two stages viz.

- 1) Single cylinder;
- 2) Two cylinders placed side by side.

In the first experiment a single, circular, brass cylinder of 25.4 mm diameter and 254 mm height was placed at the centre of the test section. The readings were recorded at six different locations with $\frac{X}{D} = 0.5, 1.0, 2.0, 3.0, 4.0$ and 5.0 behind the cylinder, X being measured from the downstream edge of the cylinder. Daily temperature and initial readings of the anemometer and Traversing mechanism were noted each time the experiment was conducted. A constant dial setting corresponding to a free stream velocity of 3.28 m/sec was used. A constant over heat ratio of 1.5 was maintained throughout the experiment by checking the cold resistance

and adjusting the operating resistance accordingly.

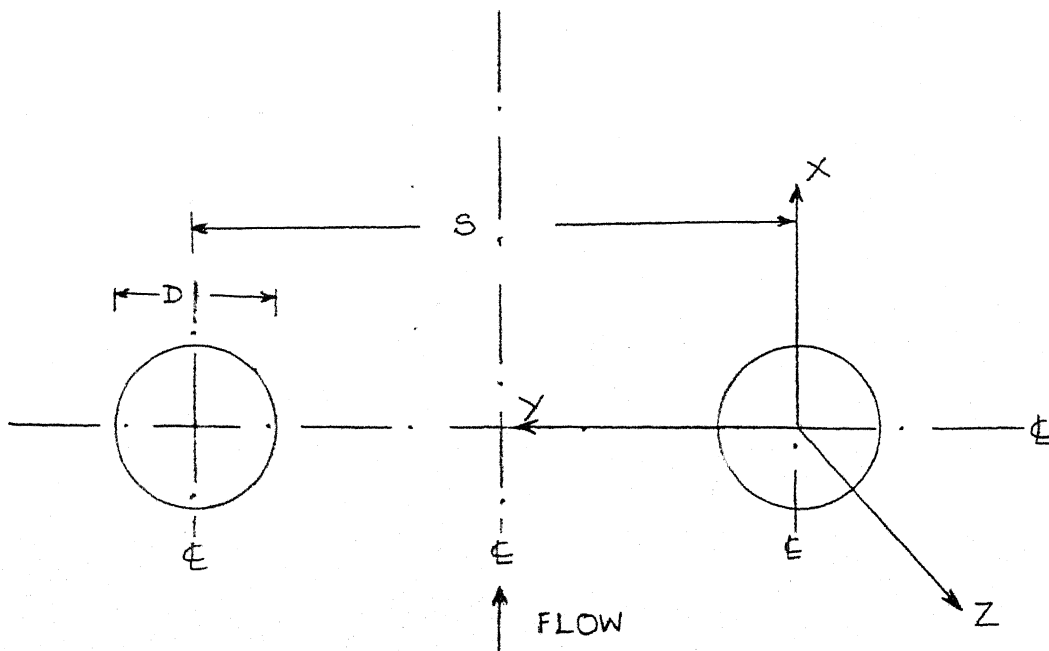
After the flow stabilised, the probe was brought behind the centre of the cylinder at $\frac{X}{D} = 0.5$. It was traversed in the Z (vertical) direction with it's initial position about 0.05 mm from the floor of the test section. Smaller intervals were used in the beginning and were increased gradually till a constant reading was observed. The readings from the RMS voltmeter and digital voltmeter were noted each time. The probe was traversed upto $\frac{Z}{D} = 1.0$ in all the cases as the readings remain constant with further increase in height. The probe is now traversed along the Y-direction at 1 mm above the floor. The smaller intervals were used in the beginning and were increased gradually till $\frac{Y}{D} = 2.0$ is reached. The probe is again traversed in the vertical direction (Z-direction) at $\frac{Y}{D} = 1.0$. The procedure was repeated for $\frac{X}{D} = 1.0, 2.0, 3.0, 4.0$ and 5.0 .

In the second set of experiments, two brass circular cylinders each of 25.4 mm diameter and 254 mm height were used for lateral spacings (in Y-direction), $\frac{S}{D} = 5.0, 7.0$ and 9.0 . First, a centre line was marked along the flow direction on the floor of the test section. From this line, points were marked on either side so that the dimensionless spacings will be 5.0, 7.0 and 9.0 respectively. These points indicate the location

of the cylinders. Holes were drilled through these points, and the cylinders were bolted for the first spacing $\frac{S}{D} = 5.0$. Now, the probe was brought behind the centre of one cylinder. It was positioned at $\frac{X}{D} = 0.5$ from the downstream edge of the cylinder. It was traversed in the vertical direction upto $\frac{Z}{D} = 1.0$. Then, the probe was traversed along the Y-direction at a height of 1 mm from the floor. This was continued till the centre of the spacings (ie. $\frac{Y}{D} = 2.5$) is reached. Again, the probe was traversed in the vertical (Z) direction at the centre of spacing. The anemometer readings were noted in each case. The procedure was repeated for different longitudinal locations, at $\frac{X}{D} = 1.0, 2.0, 3.0, 4.0$ and 5.0 . The anemometer readings were recorded each time.

Table 4.1 : Summary of experimental variables.

<u>Variable</u>	<u>Symbol</u>	<u>Range/Mean value</u>
Dimension of the test section.	-	1016mmx405mmx305mm
Free-stream velocity	U_o	3.28 m/sec
B.L. thickness	δ	12. mm
Cylinder diameter	D	25.4 mm
Cylinder height		254 mm
Cylinder spacing(lateral)	S	5D, 7D, 9D & ∞
Pier Reynold's number	R_{ep}	5250 (mean)
Velocities measured in		
(a) Main-stream direction	X	0.50D to 5D
(b) Lateral direction	Y	0 to S/2
(c) Vertical direction	Z	0.05 mm to 25.4 mm

Fig. 4.2 : DEFINITION SKETCH SHOWING CYLINDER LOCATIONS
AND CO ORDINATE axes

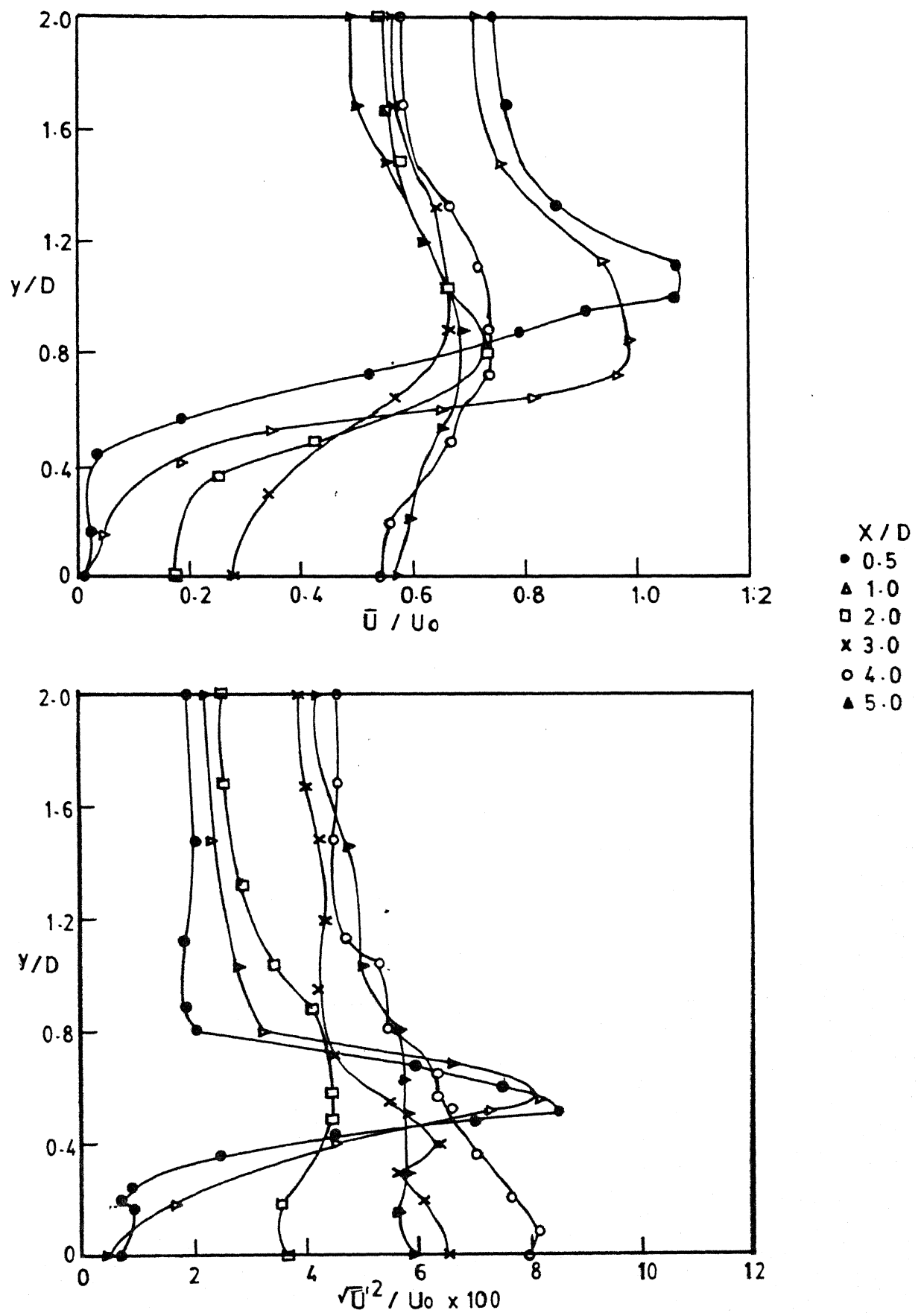
CHAPTER 5

ANALYSIS OF RESULTS AND DISCUSSIONS

In the experiments described in Chapter 4, mean and RMS velocities in the mainstream direction have been measured downstream of circular cylinders mounted side by side in steady turbulent boundary layer flow. The velocity distributions in the cartesian co-ordinate directions, namely X - longitudinal direction, Y - lateral direction and Z - vertical direction, have been compared with the velocity distributions in undisturbed boundary layer flow to understand the effect of cylindrical obstructions. Attempts have been made to delineate and study the wakes behind cylinders separately from the region outside wakes. This is necessary in order to understand the mutual interference effect of two cylinders as distinct from that of an isolated cylinder. When two cylinders were used the different spacings studied are $S/D = 5, 7$ and 9 .

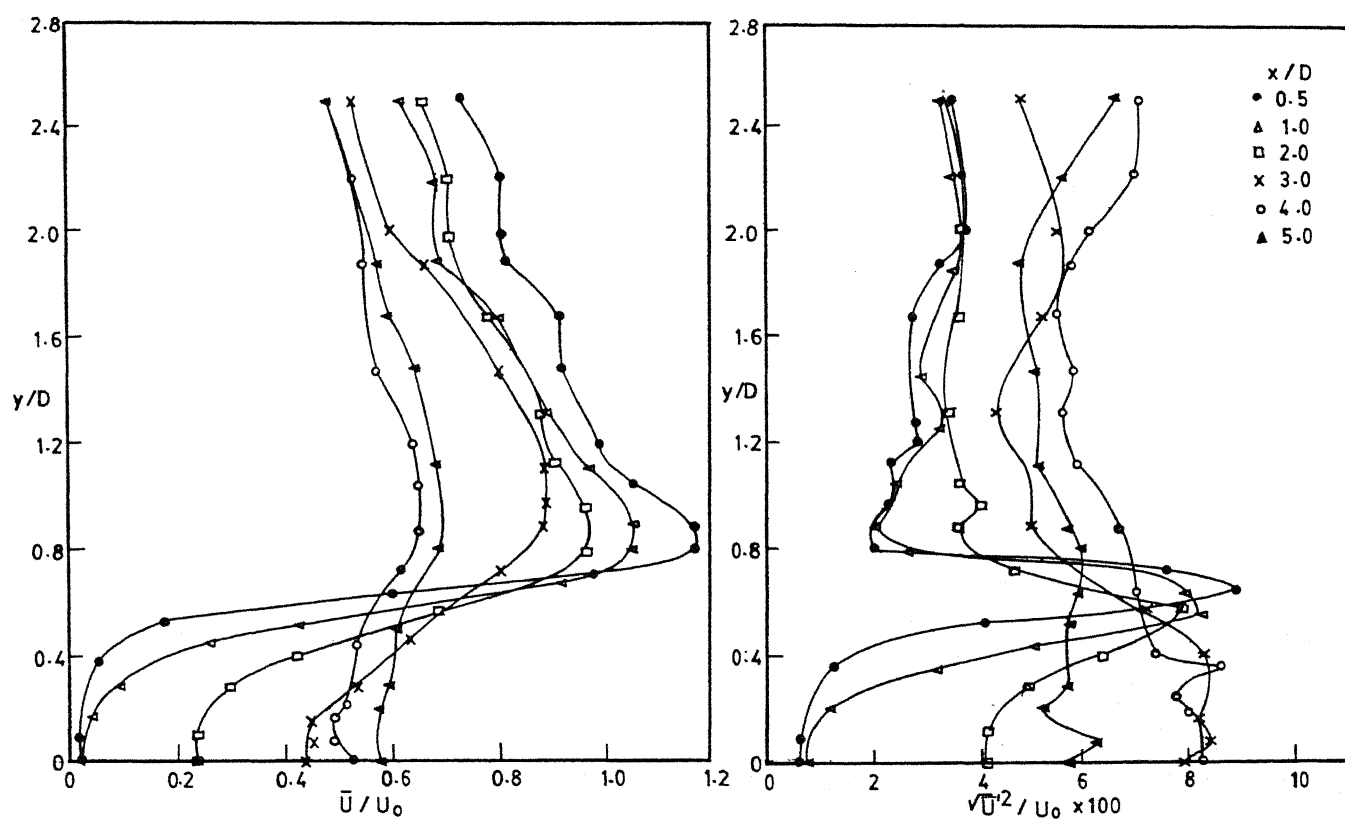
5.1 LATERAL PROFILES OF MEAN VELOCITY AND RMS VELOCITY NEAR THE WALL :

Figures 5.1, 5.2, 5.3 & 5.4 show the mean velocity profiles measured at $\frac{Z}{D} = 0.04$ in lateral direction (Y) for $\frac{X}{D} = 0.5, 1, 2, 3, 4$ & 5 and $\frac{S}{D} = 5, 7, 9$ and ∞ . It may be observed that $\frac{\bar{U}}{U_0}$ behind the centre of cylinder gradually increases in X - direction. The wake region may be demarcated



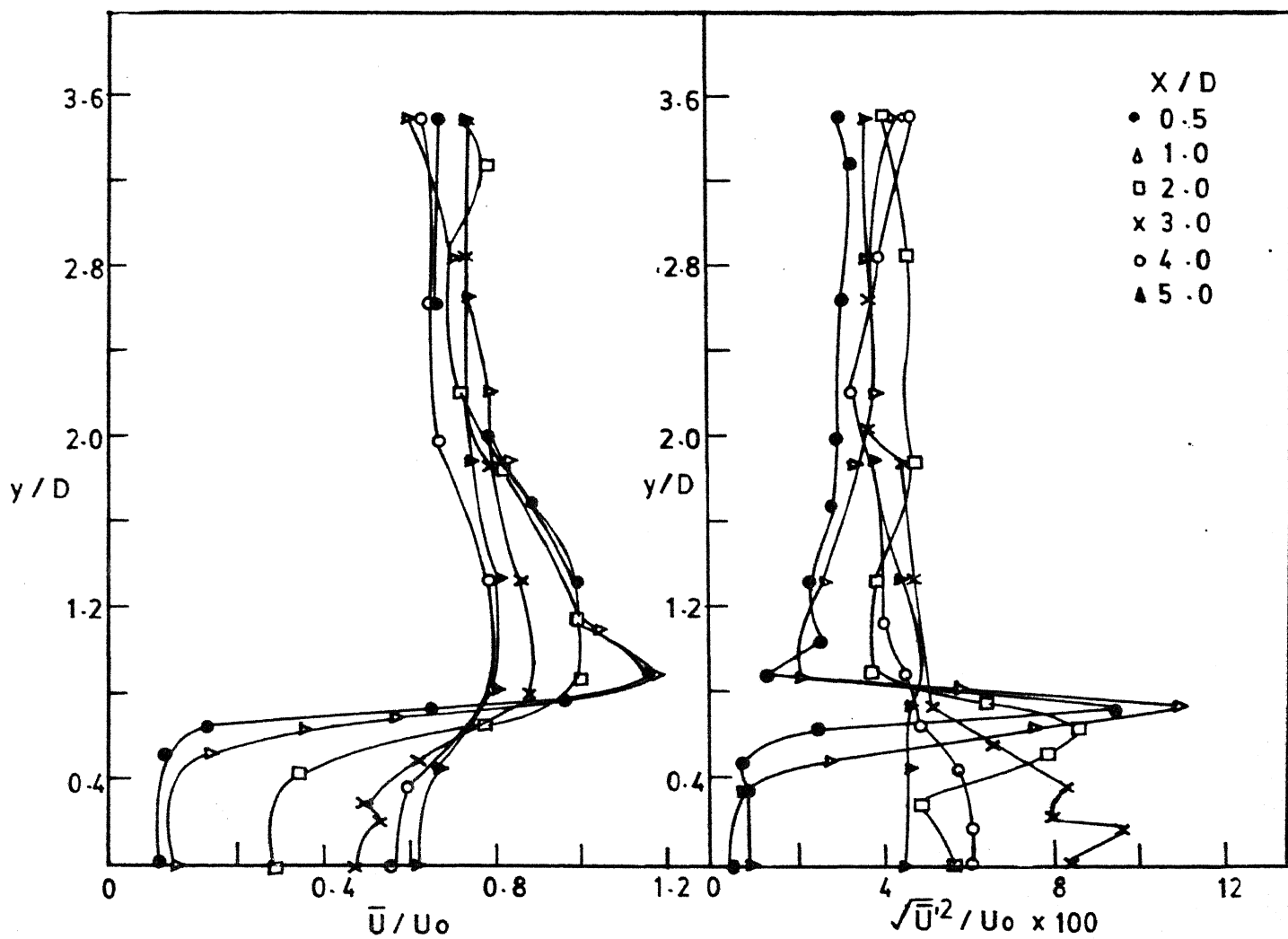
MEAN AND RMS VELOCITY PROFILES IN LATERAL DIRECTION
AT $Z/D = 0.04$ FOR $S/D = \infty$

FIG. 5-1



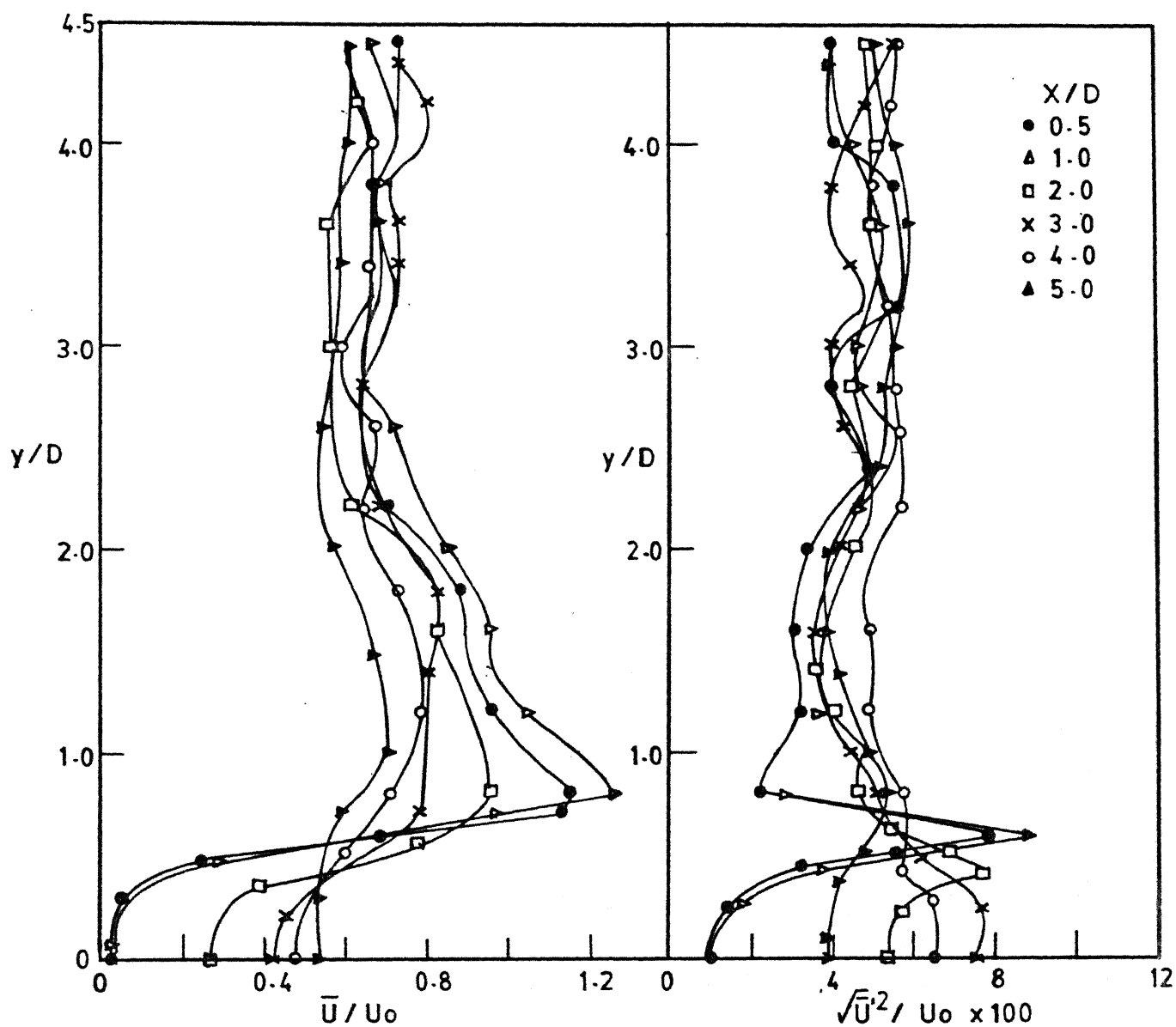
MEAN AND RMS VELOCITY PROFILES IN LATERAL DIRECTION AT $Z/D = 0.04$ FOR $S/D = 5$

FIG. 5.2



MEAN AND RMS VELOCITY PROFILES IN LATERAL DIRECTION
AT $Z/D = 0.04$ FOR $S/D = 7$

FIG. 5-3



MEAN AND RMS VELOCITY PROFILES IN LATERAL DIRECTION
AT $Z/D = 0.04$ FOR $S/D = 9$

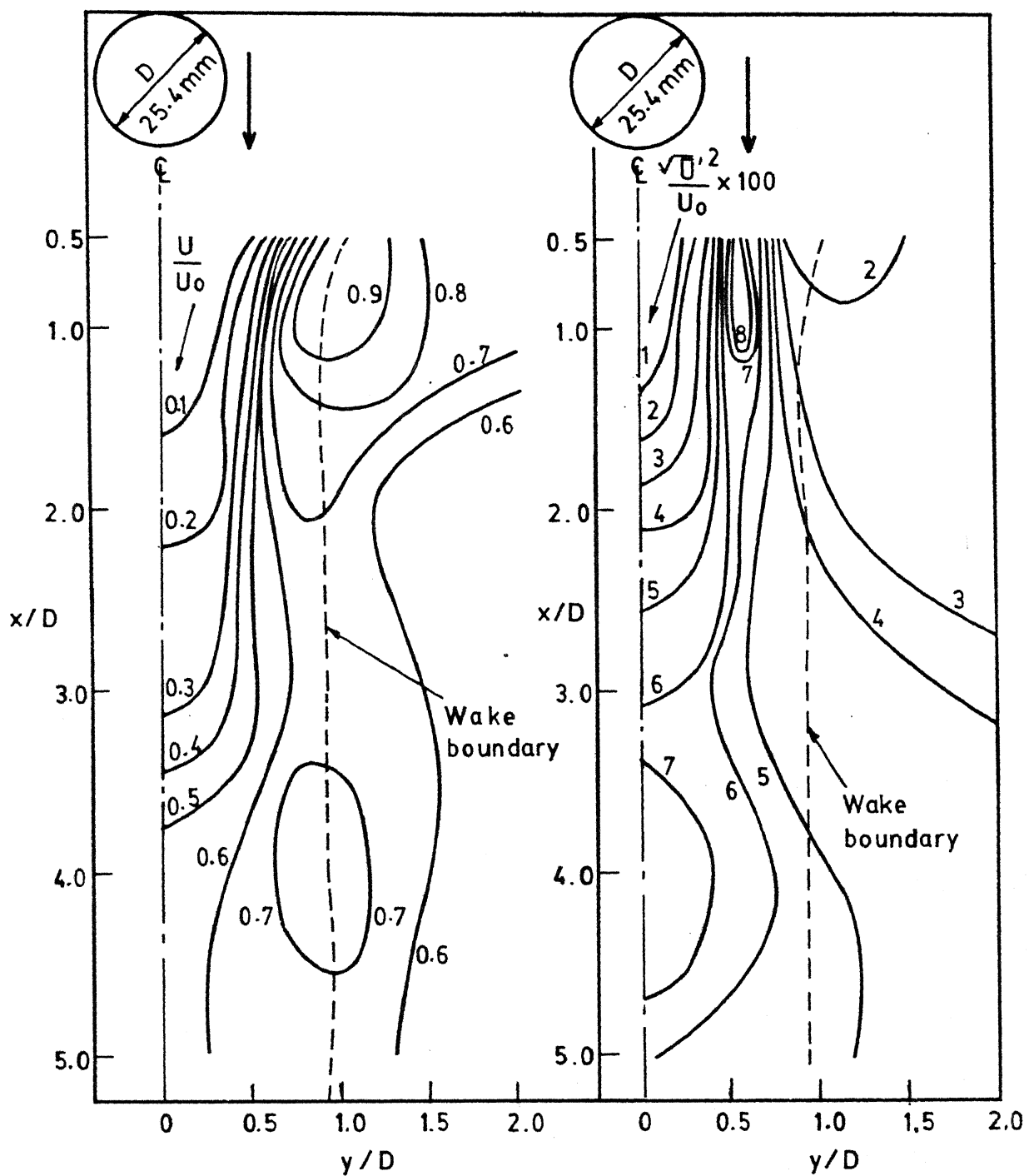
FIG. 5.4

by the maxima of $\frac{\bar{U}}{\bar{U}_0}$ in the lateral profile. The velocity distribution in the wake region gradually increases with Y attains a maximum and then decreases gradually. This trend is observed for all the cases.

Based on these mean velocity profiles, near the bed, mean velocity contours have been drawn for $\frac{S}{D} = 5, 7, 9 \text{ \& } \infty$. The edge of the wake has been indicated in Figs. 5.5 through 5.8. It may be observed that the velocity gradually increases in the wake region. At the outer edge of the wake region upto the centre of the spacing no systematic variation in the mean velocity is observed.

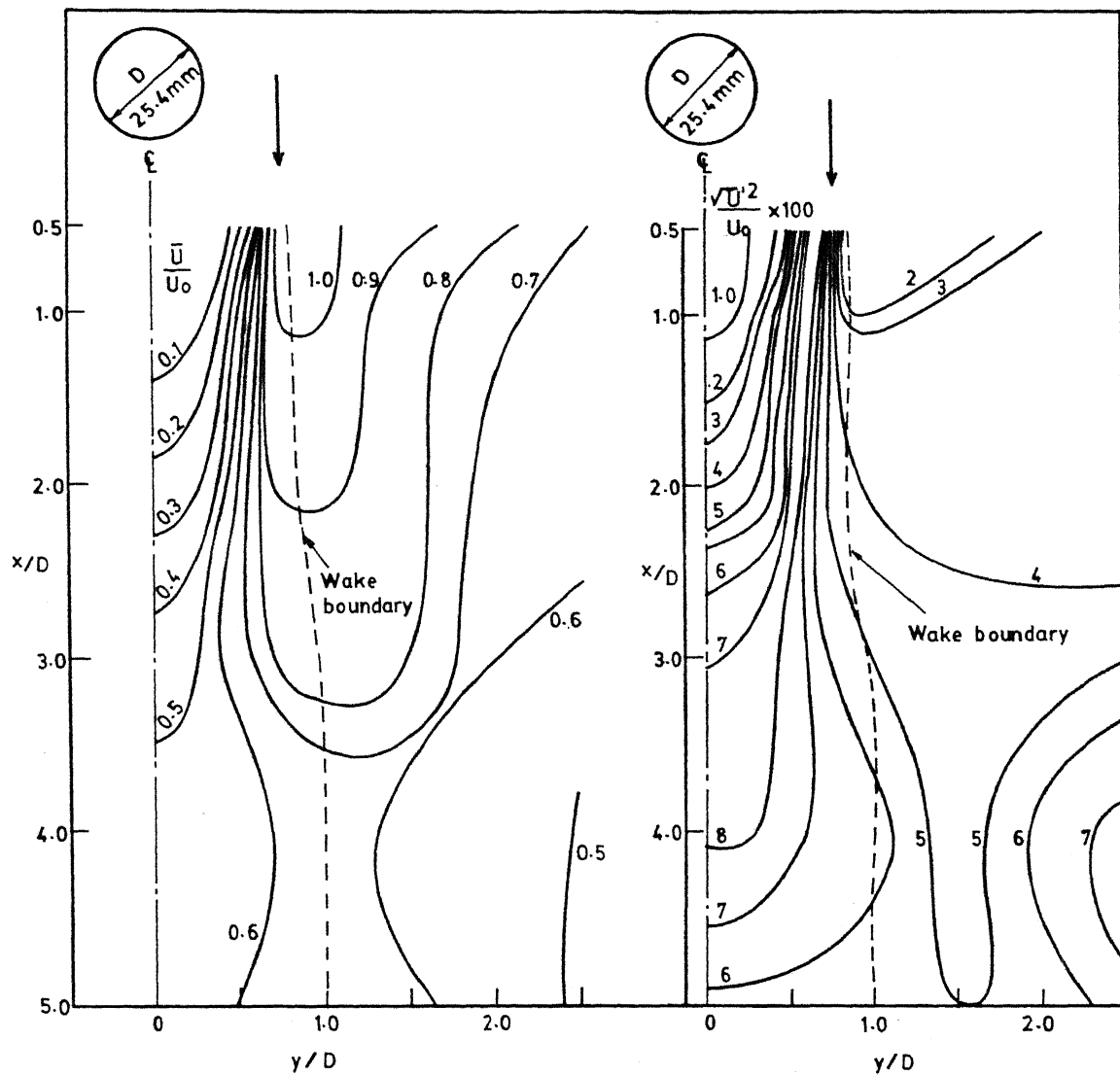
Figures 5.1, 5.2, 5.3 & 5.4 also show the RMS velocity $(\frac{\sqrt{\bar{U}^2}}{\bar{U}_0} \times 100)$ profiles at $\frac{Z}{D} = 0.04$ in lateral direction for $\frac{X}{D} = 0.5, 1, 2, 3, 4 \text{ \& } 5$ and $\frac{S}{D} = 5, 7, 9 \text{ \& } \infty$. The RMS velocity increases very steeply from $Y = 0$ towards the edge of the wake, then decreases sharply and levels off at $Y = \frac{S}{2}$. The steep increase in RMS velocity near the edges of the wake gradually decreases with increase in $\frac{X}{D}$. The RMS velocity along $Y = 0$ gradually increases in the X - direction.

Based on the above profiles, RMS velocity contours have been drawn for $\frac{S}{D} = 5, 7, 9 \text{ \& } \infty$. The edge of the wake developed from the mean velocity criteria is indicated in

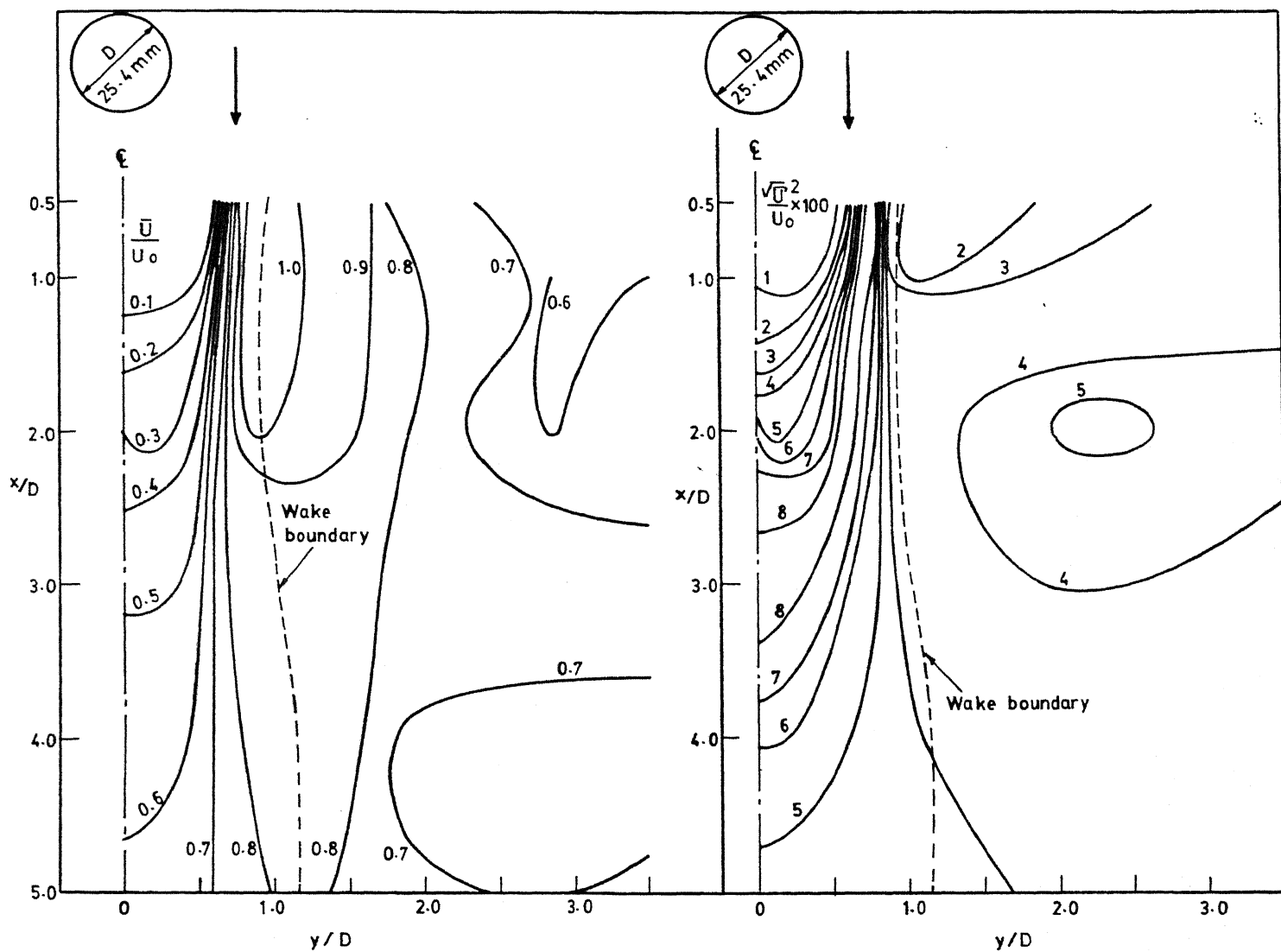


MEAN AND R.M.S. VELOCITY CONTOURS FOR $S/D = \infty$ AT $Z/D = 0.04$

FIG. 5.5

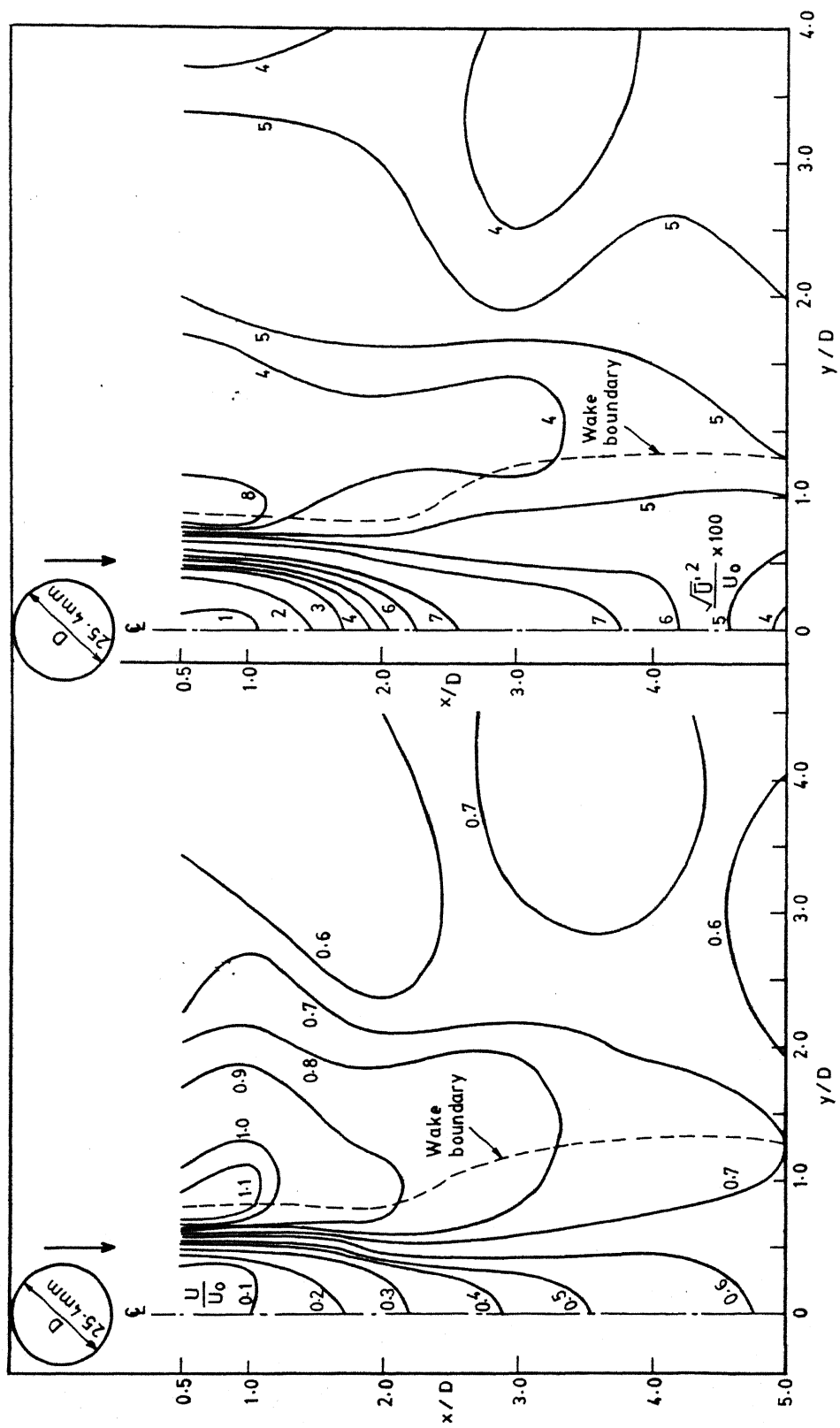


MEAN AND R.M.S. VELOCITY CONTOURS FOR $S/D=5$ AT $Z/D=0.04$
FIG. 5-6



MEAN AND R.M.S. VELOCITY CONTOURS FOR $S/D = 7$ AT $Z/D = 0.04$

FIG. 5.7



MEAN AND R.M.S. VELOCITY CONTOURS FOR $S/D = 9$ AT $Z/D = 0.04$

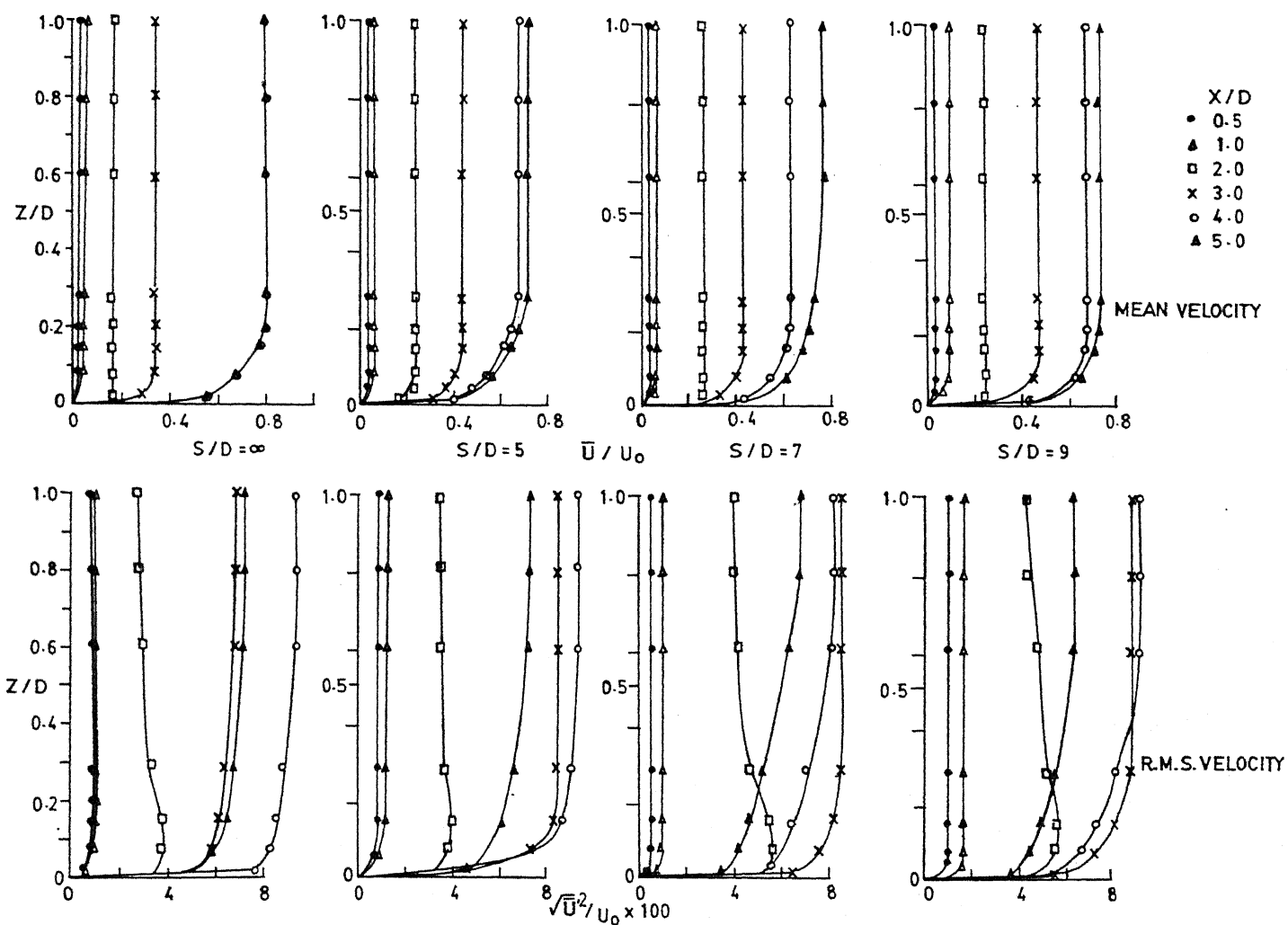
FIG. 5-8

Figs. 5.5 through 5.8. It may be observed that the RMS velocity gradually increases and then starts decreasing with increase in $\frac{X}{D}$ along $Y = 0$. However, there is no systematic variation in the region between the edge of the wake and the plane $Y = \frac{S}{2}$.

5.7 VERTICAL PROFILES OF MEAN VELOCITY AND RMS VELOCITY :

The vertical profiles of mean velocity for various values of $\frac{X}{D}$ and for $\frac{S}{D} = 5, 7, 9$ and are shown in Figs. 5.9 & 5.10. The mean velocity profiles along $Y = 0$ gradually increase near the wall and remain fairly constant for higher values of $\frac{Z}{D}$. The region of increase in mean velocity profile can be considered as the zone in which wall effect is significant. At $Y = 0$, the dimensionless maximum velocity $\frac{\bar{U}}{U_0}$ is plotted against $\frac{X}{D}$ for $\frac{S}{D} = 5, 7, 9$ & . It may be observed that $\frac{\bar{U}}{U_0}$ increases gradually with increase in $\frac{X}{D}$. The position ($\frac{Z}{D}$) at which the maximum velocity occurs, is plotted against $\frac{X}{D}$ for $\frac{S}{D} = 5, 7, 9$ & . It is observed that, $\frac{Z}{D}$ tends to decrease upto $\frac{X}{D} = 2.0$ and then increases for $\frac{X}{D} > 2.0$.

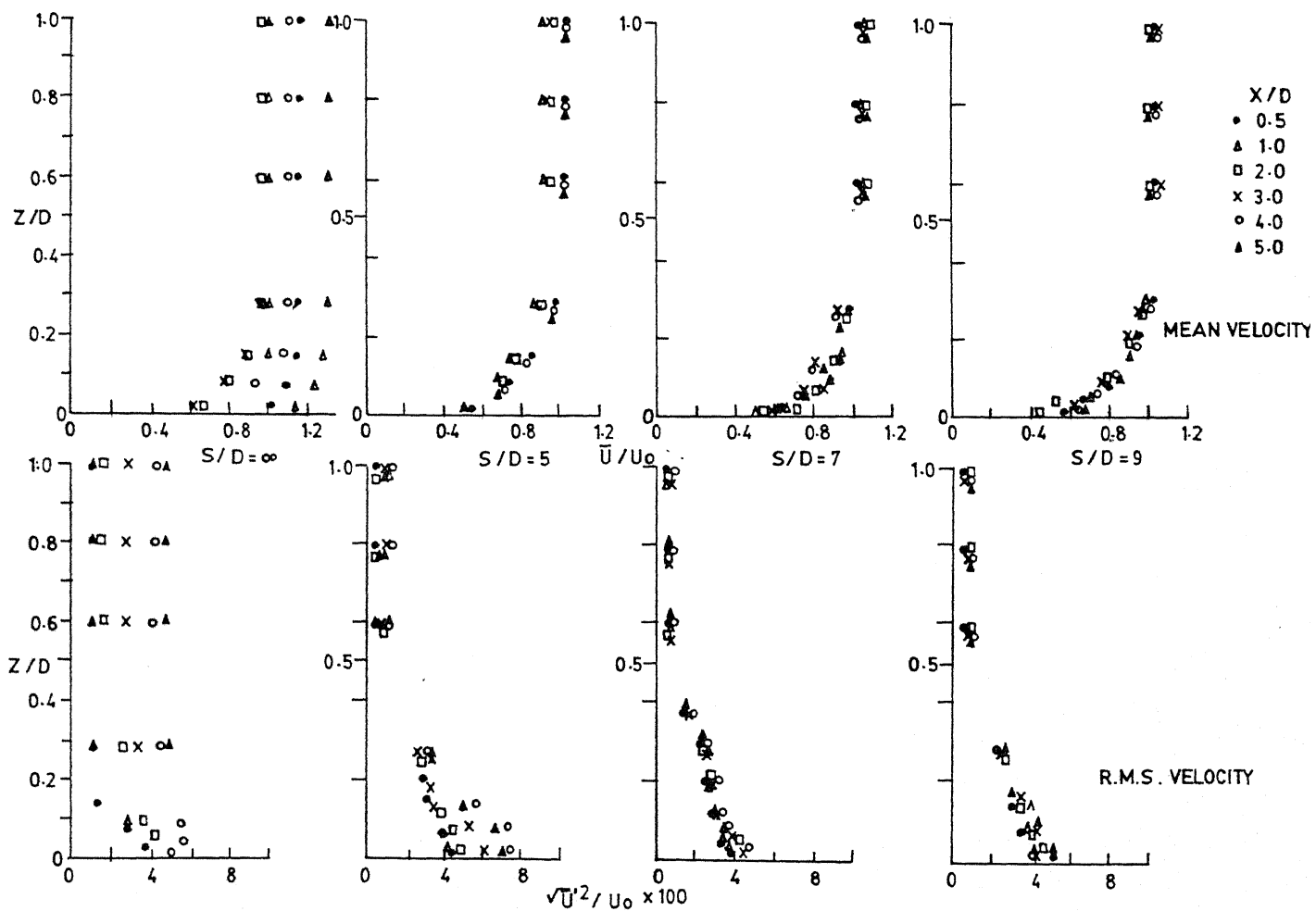
Vertical profiles of $\frac{\bar{U}}{U_0}$ along $Y = \frac{S}{2}$ are plotted for different values of $\frac{X}{D}$ and $\frac{S}{D}$ as shown in Fig. 5.10. It may be observed that they are similar to boundary layer velocity profiles. The maximum dimensionless velocity $\frac{U_{se}}{U_0}$ given by these profiles is plotted against $\frac{X}{D}$ for different $\frac{S}{D}$ values. It may be observed that there is a slight increase in maximum



Mean and R.M.S. velocity distribution in vertical direction along the centre line behind the cylinder

FIG. 5.9

CENTRAL LIBRARY
I. I. T. KANPUR
Acc. No. A107868

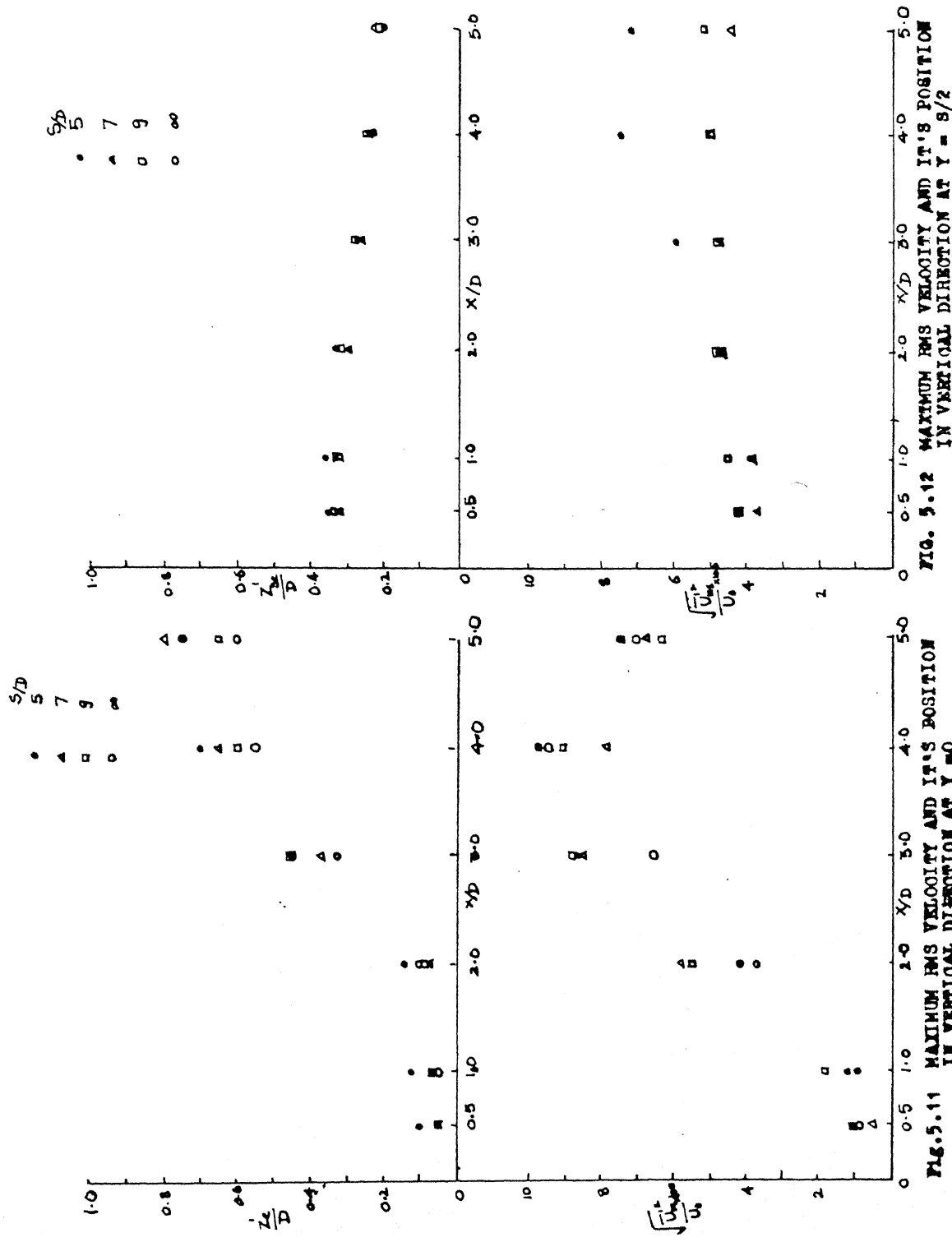


MEAN AND R.M.S VELOCITY DISTRIBUTION IN VERTICAL DIRECTION ALONG THE CENTRE LINE
IN BETWEEN THE CYLINDERS

FIG. 5-10

velocity upto $\frac{X}{D} = 2.0$ and then reduces gradually to free stream velocity for higher $\frac{X}{D}$ values. The position $\frac{z_{se}}{D}$, at which $\frac{\bar{U}_{se}}{U_o}$ occurs is plotted against $\frac{X}{D}$ for different values of $\frac{S}{D}$. It can be seen that $\frac{z_{se}}{D}$ gradually increases with $\frac{X}{D}$.

R.M.S. velocity profiles in vertical direction for various values of $\frac{X}{D}$ and $\frac{S}{D} = 5, 7, 9 \text{ \& } \infty$ are shown in Figures 5.9 & 5.10. Along $Y = 0$, the RMS velocity increases gradually upto $Z = Z'e$ and remains fairly constant for $Z > Z'e$. In vertical profile the RMS velocity along $Y = \frac{S}{2}$ increases steeply near the wall upto $\frac{Z}{D} = 0.04$ and decreases for higher values of $\frac{Z}{D}$ indicating similarity with turbulent boundary layer of mean velocity. Fig. 5.11 shows the maximum RMS velocity along $Y = 0$ plotted against $\frac{X}{D}$. It may be observed that value of RMS velocity increases upto $\frac{X}{D} = 4$ and tends to decrease with further increase in $\frac{X}{D}$. The position $(\frac{Z'e}{D})$ at which the maximum value of RMS velocity occurs is plotted against $\frac{X}{D}$ for various values of $\frac{S}{D}$. It may be observed that $\frac{Z'e}{D}$ increases first gradually upto $\frac{X}{D} = 2.0$ and then steeply for higher values of $\frac{X}{D}$. The maximum RMS velocity $\sqrt{\frac{\bar{U}_{ms}^2}{U_o^2}}$, along $Y = \frac{S}{2}$ is plotted against $\frac{X}{D}$ as shown in Fig. 5.12. It is observed that $\sqrt{\frac{\bar{U}_{ms}^2}{U_o^2}}$ increases gradually with $\frac{X}{D}$ upto $\frac{X}{D} = 4.0$ and then starts decreasing. The position $\frac{Z'_{50}}{D}$ at which 50% of the maximum RMS velocity occurs is plotted against $\frac{X}{D}$ (Fig. 5.12). It is observed that this position gradually decreases with $\frac{X}{D}$.



5.3 VARIATION OF RMS VELOCITY AT THE EDGE OF THE WAKE :

The edge of the wake is indicated by the maximum mean velocity in lateral direction. The RMS velocity at the edge of the wake is plotted against $\frac{X}{D}$ for different values of $\frac{S}{D}$ as shown in Fig. 5.13. It may be observed that the RMS velocity increases with $\frac{X}{D}$. The effect of interference is indicated by the maximum value of RMS velocity at $\frac{X}{D} = 4$ & 5 for decreasing $\frac{S}{D}$ values.

The maximum values of RMS velocity in the lateral direction $\sqrt{\frac{\bar{U}^2_{max}}{\bar{U}^2_0}}$ at $\frac{S}{D} = 0.04$ is plotted against $\frac{X}{D}$ for all $\frac{S}{D}$ as shown in Fig. 5.13. $\sqrt{\frac{\bar{U}^2_{max}}{\bar{U}^2_0}}$ decreases fairly upto $\frac{X}{D} = 2.0$, then increases gradually for $\frac{X}{D} = 3$ to 4, and decreases again for higher values of $\frac{X}{D}$. The magnitude of $\sqrt{\frac{\bar{U}^2_{max}}{\bar{U}^2_0}}$ is high for smaller values of $\frac{S}{D}$ and decreases with increase in $\frac{S}{D}$. The position $\frac{Y'}{D}$, at which $\sqrt{\frac{\bar{U}^2_{max}}{\bar{U}^2_0}}$ occurs is plotted against $\frac{X}{D}$. It is observed that Y'/D gradually decreases with increase in $\frac{X}{D}$ and is almost zero for $\frac{X}{D} \geq 5$.

5.4 COMPARISON OF RMS VELOCITY PROFILES AT THE CENTRE, EDGE AND OUTSIDE THE WAKE REGION :

RMS velocity profiles for different values of $\frac{X}{D}$ in the centre line, edge and outside the wake region where $\frac{Y}{D} = 1$ are shown in Fig. 5.14. The RMS velocity at the edge of the wake is much higher for $\frac{X}{D} = 0.5$ in comparison with the centre

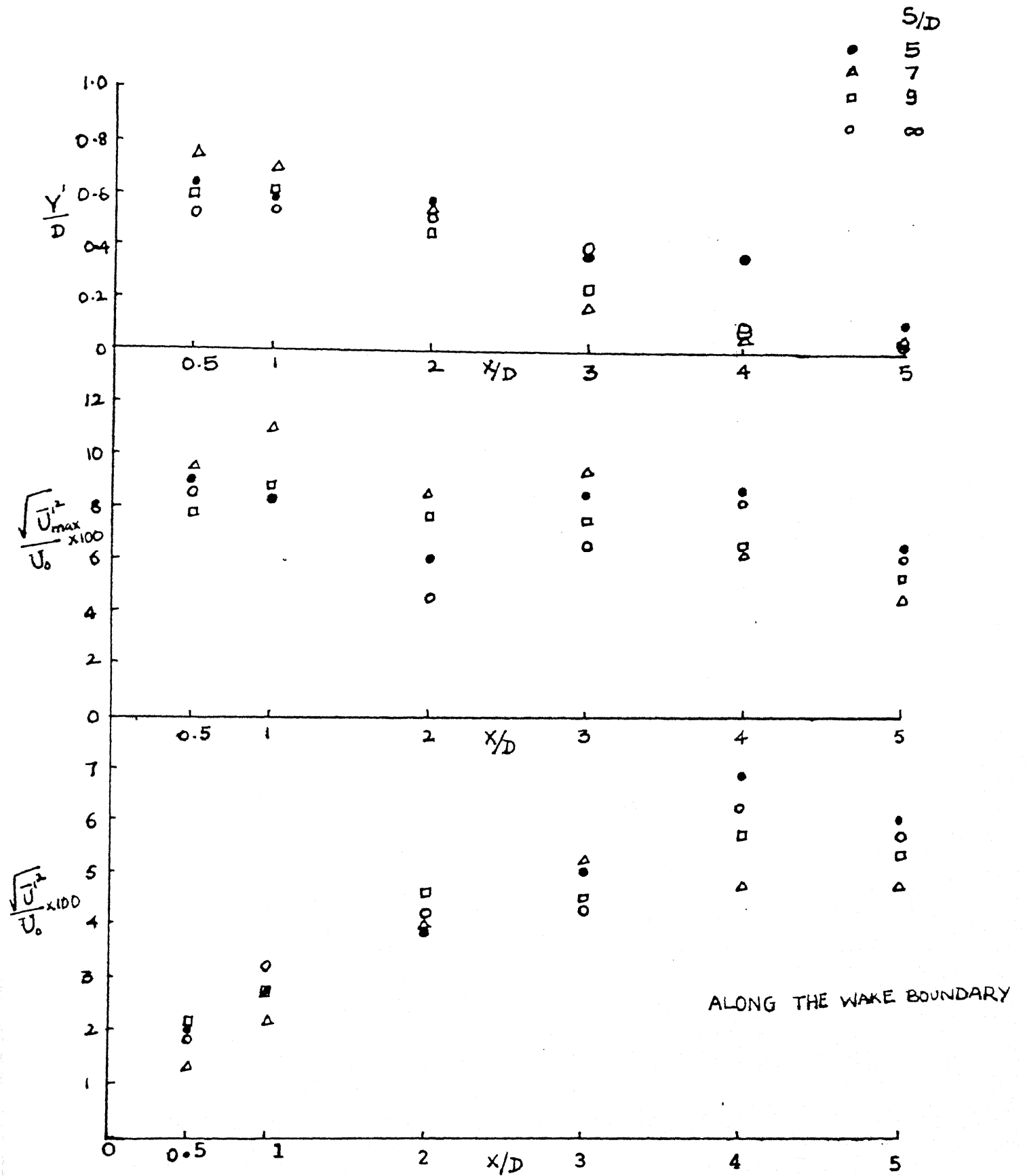
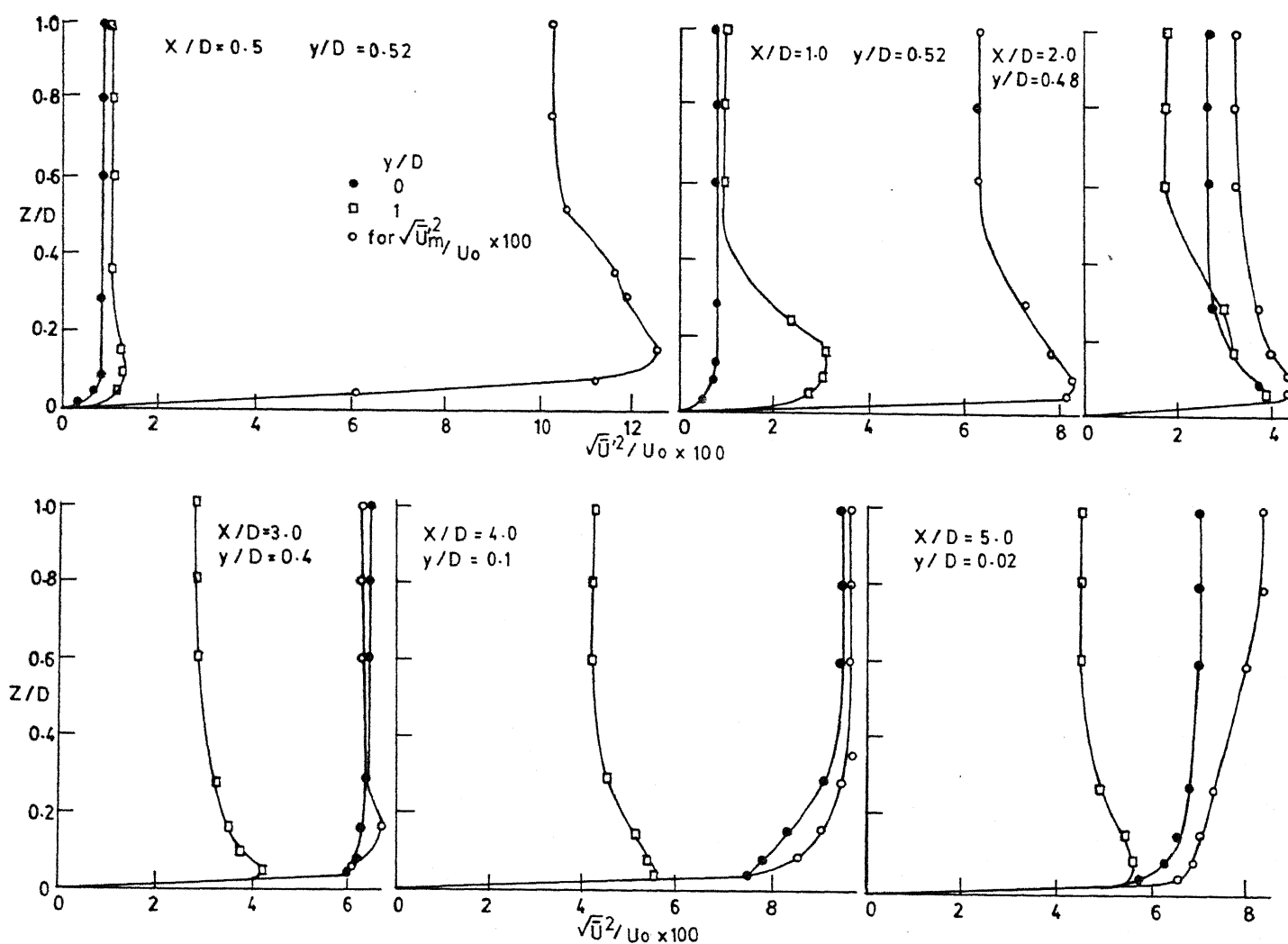


FIG. 5.13 : LONGITUDINAL VARIATION OF $\frac{\sqrt{U^2}}{U_0} \times 100$, $\frac{\sqrt{U_{max}^2}}{U_0} \times 100$, $\frac{Y'}{D}$ AT $\frac{Z}{D} = 0.04$.



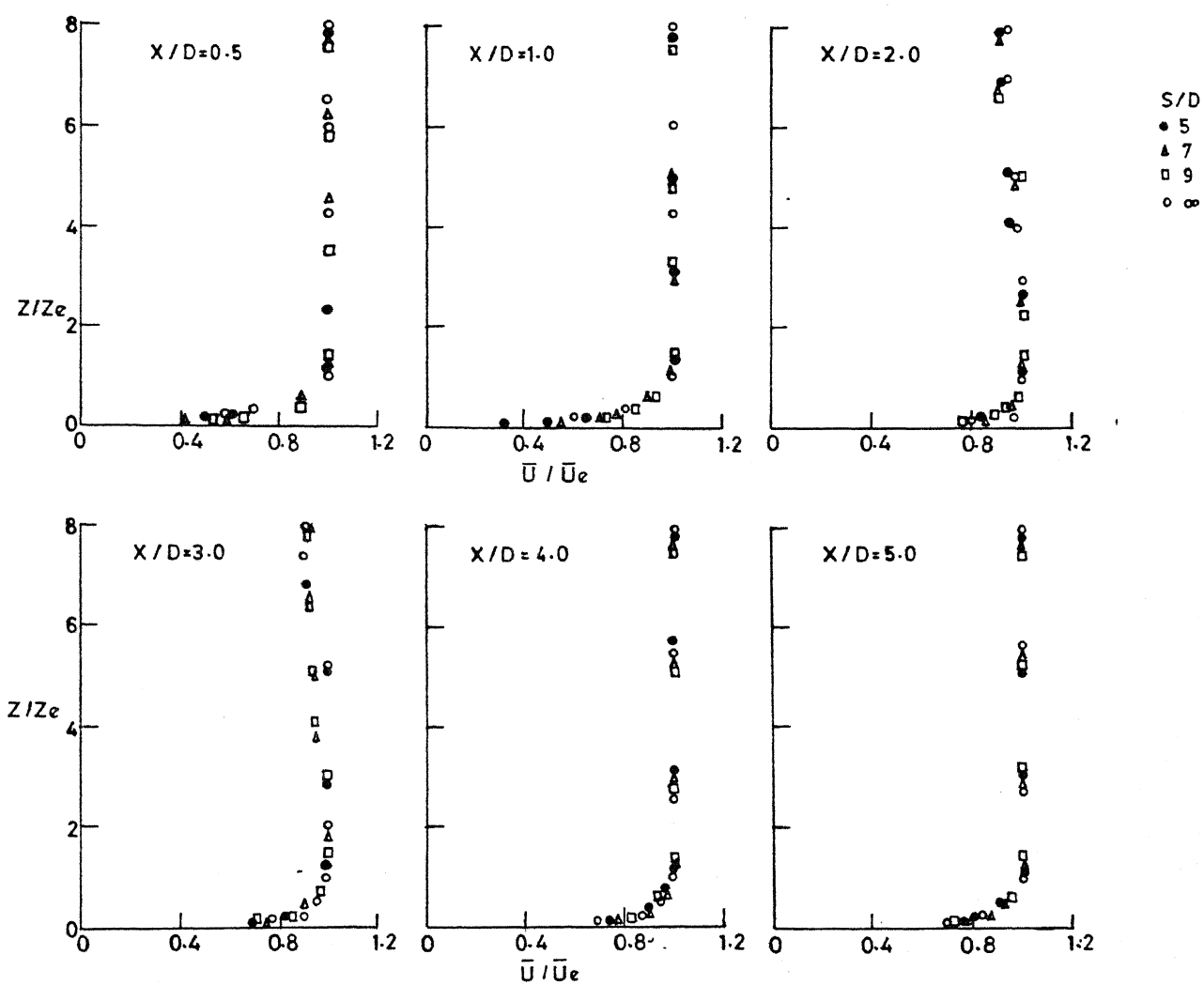
VERTICAL PROFILES OF RMS VELOCITY IN THE CENTRE EDGE AND OUTSIDE THE WAKE REGION

FIG. 5-14

line and outer region velocities for all $\frac{Z}{D}$. However, as $\sqrt{\frac{\bar{U}^2}{U_o}}$ at the wake edge decreases with $\frac{X}{D}$, at $\frac{X}{D} = 2.0$ all the three $\sqrt{\frac{\bar{U}^2}{U_o}}$ profiles come close to each other. For $\frac{X}{D} = 3$ the centre line and edge profiles nearly coincide whereas they don't quite match with the profile for outer region ($\frac{Y}{D} = 1.0$). From the observations, it is clear that the effect of wake on $\sqrt{\frac{\bar{U}^2}{U_o}}$ is more predominant at the boundary for small values of $\frac{X}{D}$.

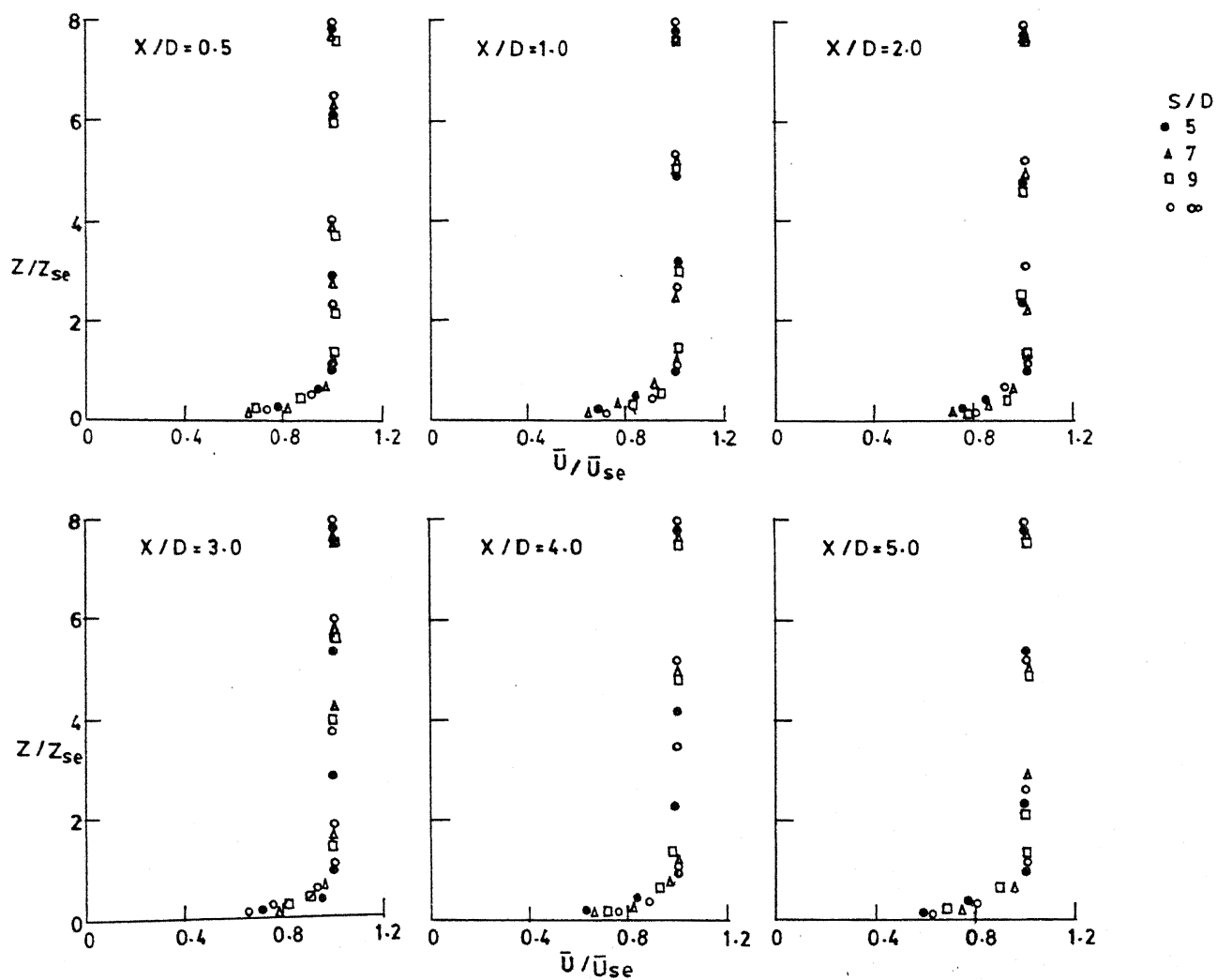
5.5 MEAN VELOCITY DISTRIBUTION IN THE VERTICAL DIRECTION :

Mean velocity is found to gradually increase from the wall to a height designated Z_e in the wake zone and Z_{se} outside the wake zone. The velocity profiles drawn for different values of $\frac{X}{D}$ and $\frac{S}{D}$ are shown in Figs. 5.9 & 5.10. The velocity distribution in the wall affected zone at different $\frac{X}{D}$ using the power law as $\frac{\bar{U}}{U_e} = \left(\frac{Z}{Z_e}\right)^{1/n}$ for $Y = 0$ and $\frac{\bar{U}}{U_{se}} = \left(\frac{Z}{Z_{se}}\right)^{1/n}$ for $Y = \frac{S}{2}$ in the flow direction are shown in Figs. 5.15 & 5.16. It may be observed that the power law agrees fairly with the experimental data for different values of 'n'. The exponent 'n' plotted against $\frac{X}{D}$ for $Y = 0$ and $\frac{S}{2}$ respectively in Fig. 5.15 is seen to increase steeply upto $\frac{X}{D} = 2.0$ and decreases with further increase in $\frac{X}{D}$ for $Y = 0$; whereas at $Y = \frac{S}{2}$, it gradually



NORMALISED MEAN VELOCITY DISTRIBUTION IN VERTICAL DIRECTION BEHIND THE CYLINDER

FIG. 5.15



NORMALISED MEAN VELOCITY DISTRIBUTION IN VERTICAL DIRECTION IN BETWEEN THE CYLINDER

FIG. 5-16

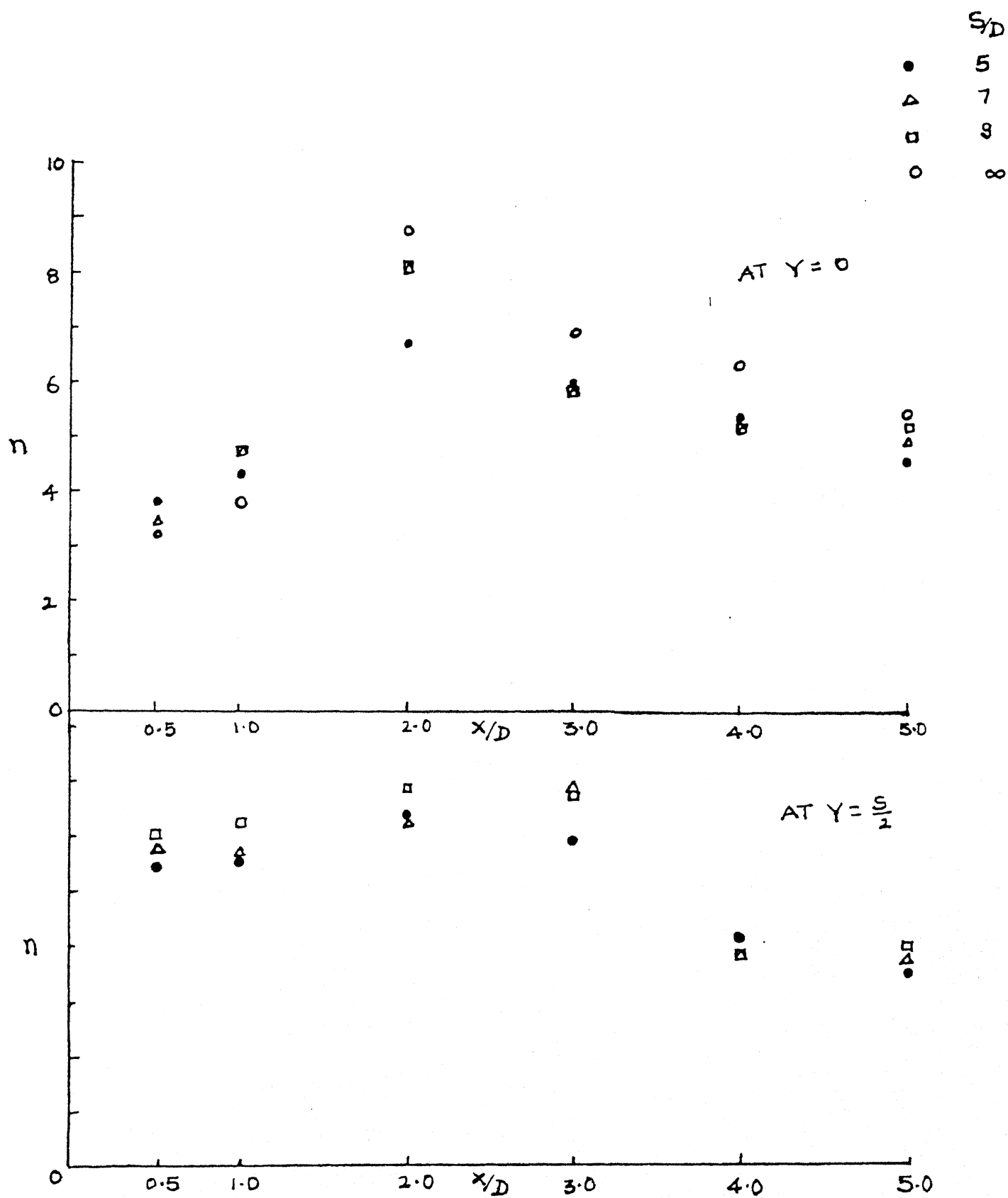


FIG. 5.17 : VARIATION OF POWER LAW EXPONENT 'n' FOR VELOCITY PROFILES.

increase upto $\frac{X}{D} = 3.0$, then decreases and attains fairly constant value for $\frac{X}{D} > 4.0$. The zone of increase in the exponent 'n' can be taken as the zone of accelerating flow. The zone of decrease in 'n' can be taken as the zone of decelerating flow. These regions can be seen in the mean velocity profiles and in the variation of exponent 'n'.

Velocity parameter $\frac{\bar{U}_e}{\bar{U}_o}$ and it's corresponding position $\frac{z_e}{D}$ along $Y = 0$, and $\frac{\bar{U}_{se}}{\bar{U}_o}$ and it's position $\frac{z_{se}}{D}$ along $Y = \frac{S}{2}$ are plotted against $\frac{X}{D}$ upto $\frac{X}{D} = 5.0$ for different values of $\frac{S}{D}$ in Figs. 5.18 and 5.19. $\frac{\bar{U}_e}{\bar{U}_o}$ is found to gradually increase with increase in $\frac{X}{D}$. The position $\frac{z_e}{D}$ at which the velocity is maximum decreases very slowly with increase in $\frac{X}{D}$, upto $\frac{X}{D} = 2.0$ and increases gradually with $\frac{X}{D} > 2.0$ as shown in the Fig. 5.18. The corresponding variations of $\frac{\bar{U}_{se}}{\bar{U}_o}$ and $\frac{z_{se}}{D}$ for flow along $Y = \frac{S}{2}$ are much less. However, $\frac{\bar{U}_{se}}{\bar{U}_o}$ is greater than 1, having a maximum value near $\frac{X}{D} = 2.0$.

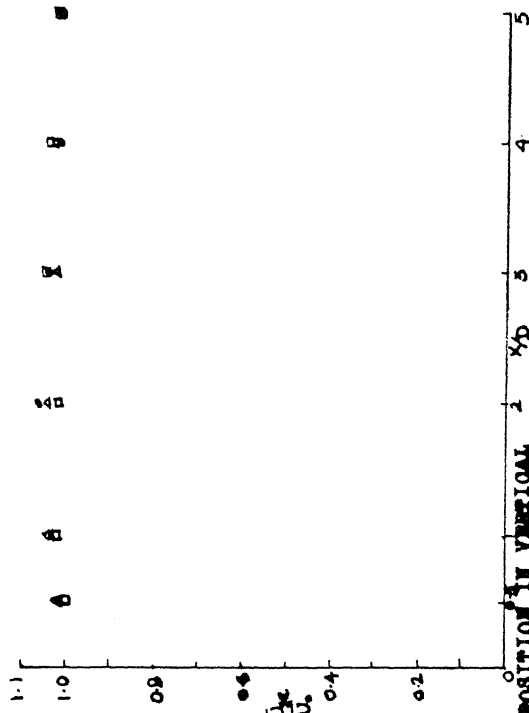
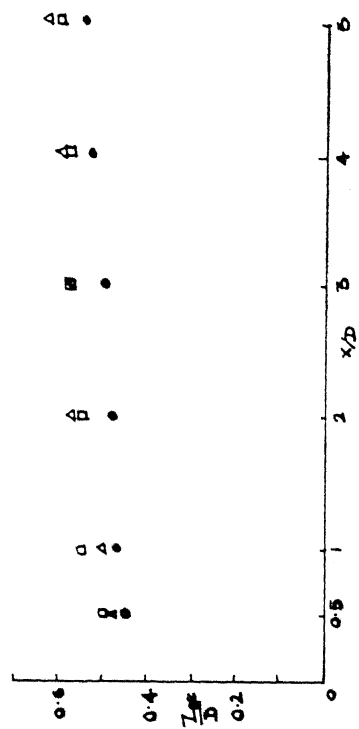
5.6 RMS VELOCITY DISTRIBUTION IN THE VERTICAL DIRECTION :

5.6.1 Behind the Cylinder ($Y = 0$) :

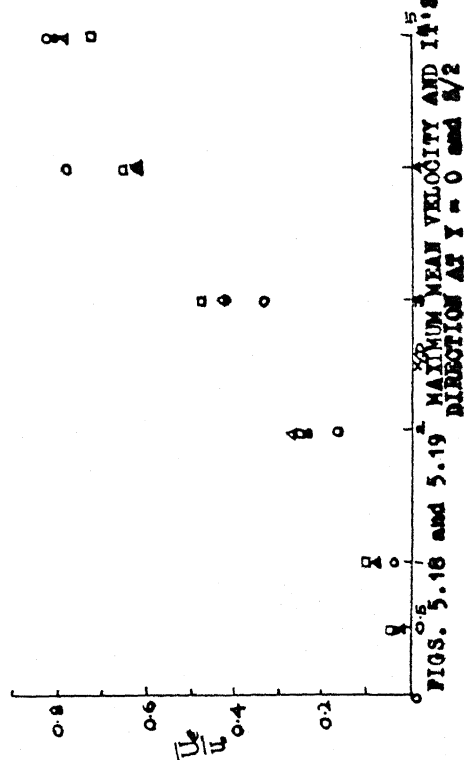
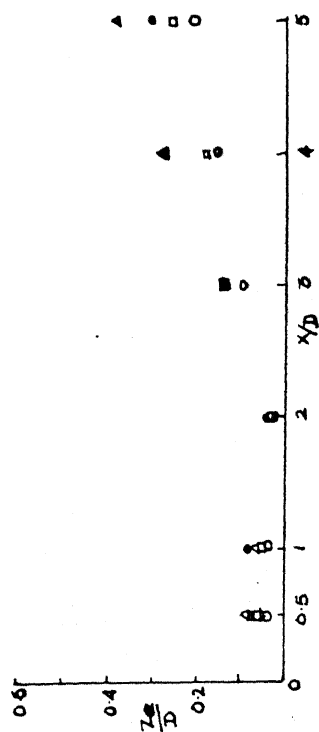
The RMS velocity profiles along $Y = 0$ non-dimensionalised as $\frac{\sqrt{\bar{U}^2}}{\sqrt{\bar{U}_m^2}}$ are plotted against $\frac{z}{z_e}$ as shown in Fig. 5.20. It may be observed that $\frac{\sqrt{\bar{U}^2}}{\sqrt{\bar{U}_m^2}}$ profiles at a given $\frac{X}{D}$ for various $\frac{S}{D}$ appear to be similar. $\frac{z_e}{D}$ gradually increases upto

SyD

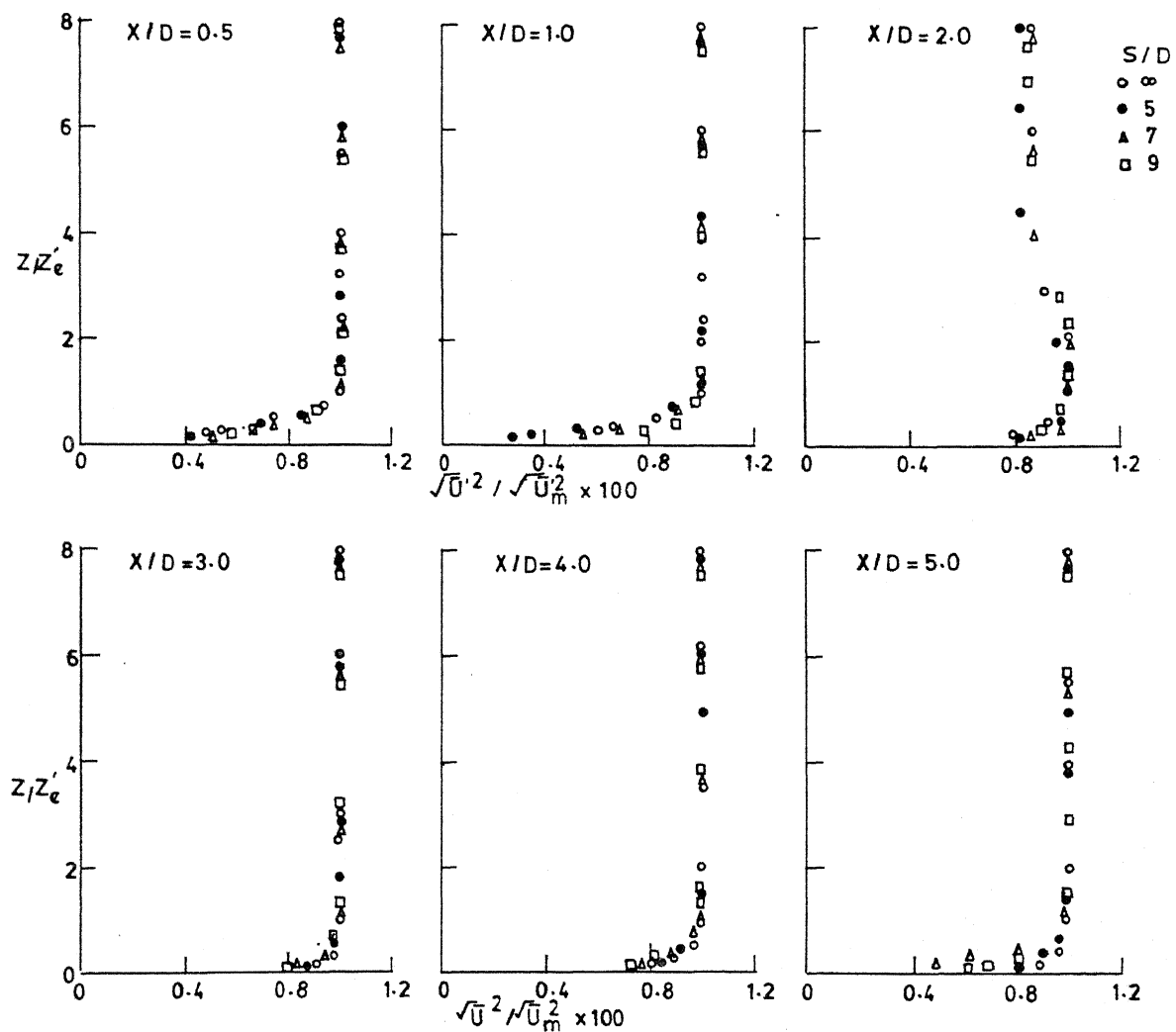
- 5
- △ 7
- 9



- 5
- △ 7
- 9
- 10



FIGS. 5.18 and 5.19 MAXIMUM MEAN VELOCITY AND 1/2 POSITION IN VERTICAL DIRECTION AT Y = 0 AND 5/2



NORMALISED RMS VELOCITY DISTRIBUTION IN VERTICAL DIRECTION BEHIND THE CYLINDER

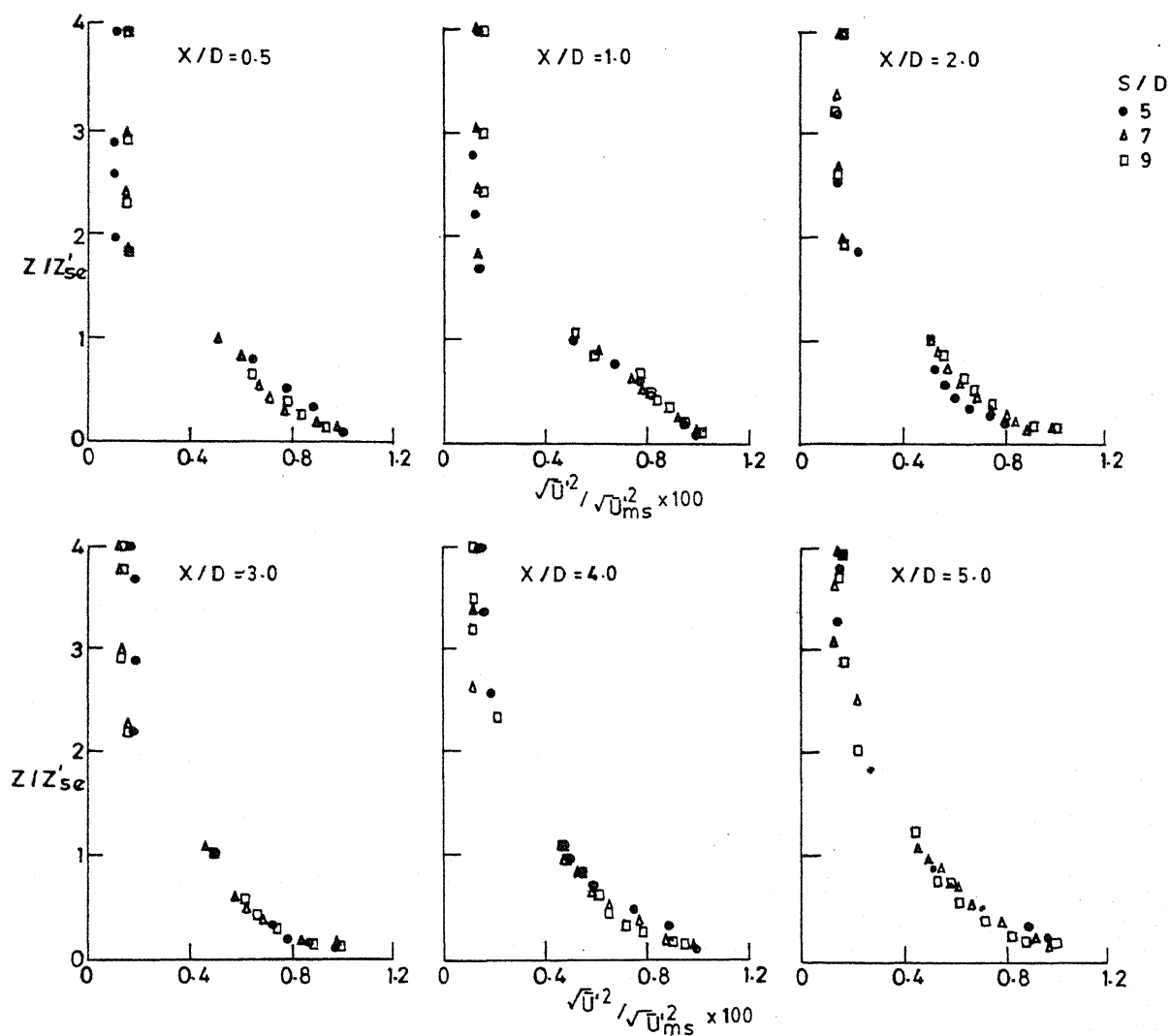
FIG. 5-20

Z' and remains fairly constant for $Z > Z'$ for all $\frac{X}{D}$ except $\frac{X}{D} = 2.0$. At $\frac{X}{D} = 2.0$, RMS velocity increases upto $Z = Z'$, then decreases upto $Z = 4Z'$ and remains constant further on.

The maximum RMS velocity $\sqrt{\frac{U_m^2}{U_o^2}}$, non-dimensionalised as $\frac{U_m}{U_o}$ and its position $\frac{Z'}{D}$ is plotted against $\frac{X}{D}$ for various values of $\frac{S}{D}$ as shown in Fig. 5.11. It may be observed that the RMS velocity parameter increases with increase in $\frac{X}{D}$ upto $\frac{X}{D} = 4.0$ and decreases further on. The maximum value of RMS velocity parameter at $\frac{X}{D} = 4$ is of the order of 10 percent of the free stream velocity. The length parameter $\frac{Z'}{D}$ increases very gradually upto $\frac{X}{D} = 2.0$ and steeply for higher values of $\frac{X}{D}$.

5.6.2 Between the Cylinders ($Y = \frac{S}{2}$) :

RMS velocity profiles non-dimensionalised as $\sqrt{\frac{U^2}{U_m^2}}$ are plotted against $\frac{Z}{Z'_{se}}$ as shown in Fig. 5.21, where Z'_{se} is the value of Z at which 50% of the maximum RMS velocity occurs. It may be observed that all the profiles coincide fairly well. The velocity parameter $\sqrt{\frac{U_m^2}{U_o^2}}$ and its position $\frac{Z'_{se}}{D}$ are plotted against $\frac{X}{D}$ in Fig. 5.13. It may be observed that increase in RMS velocity parameter with $\frac{X}{D}$ is steeper for $\frac{S}{D} = 5$ in comparison to $\frac{X}{D} = 7$ and 9. The deviation of the curve in $\frac{S}{D} = 5$ may be due to interference effects. The length



NORMALISED RMS VELOCITY DISTRIBUTION IN VERTICAL DIRECTION IN BETWEEN THE CYLINDERS

FIG. 5-21

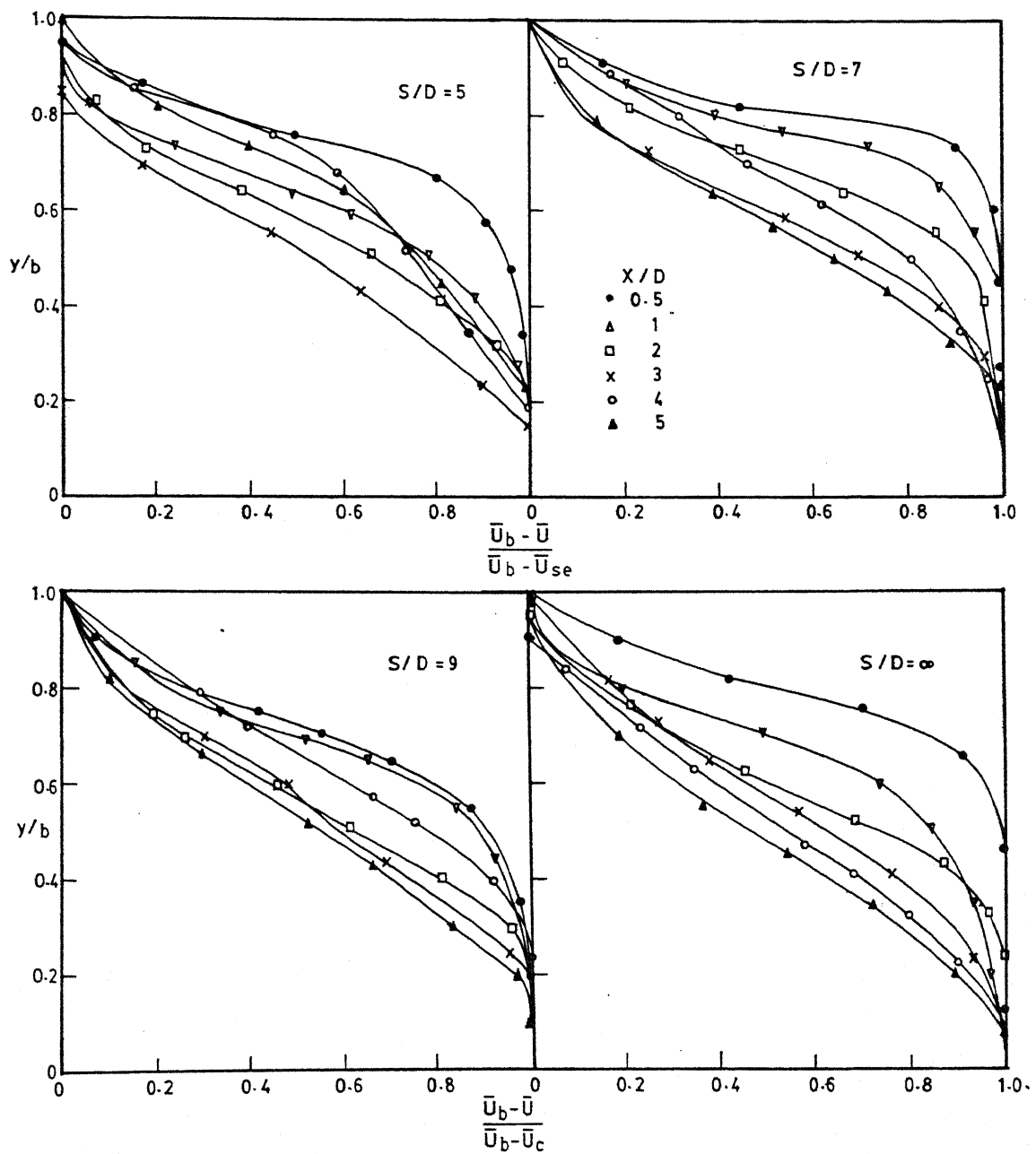
scale $\frac{z'}{D}$ decreases with increase in $\frac{X}{D}$ gradually.

5.7 MEAN VELOCITY DISTRIBUTION IN THE LATERAL DIRECTION NEAR THE WALL :

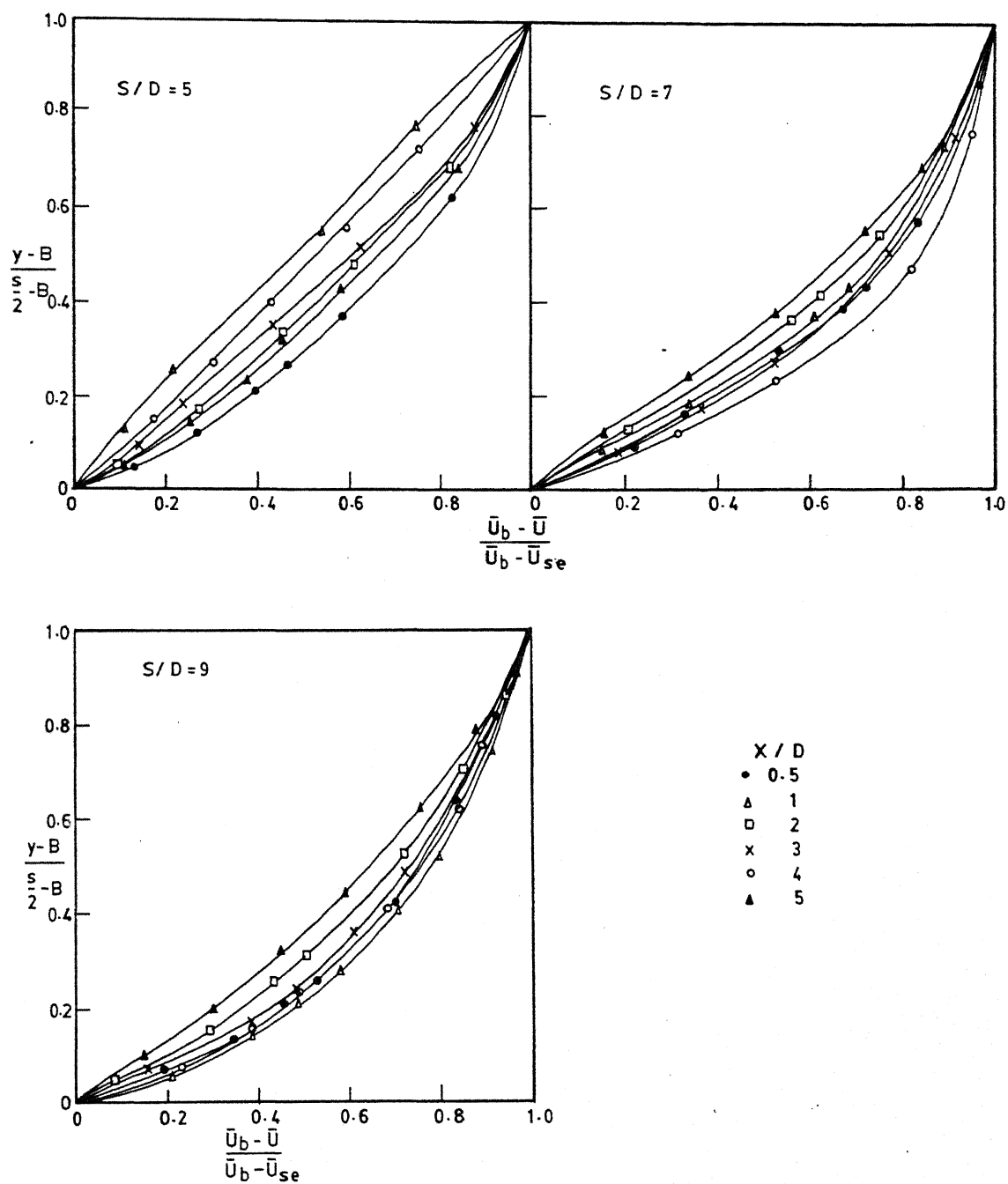
The defect in mean velocity in the wake zone at $\frac{Z}{D} = 0.04$ non-dimensionalised as $\frac{\bar{U}_b - \bar{U}}{\bar{U}_b - \bar{U}_c}$ is plotted against Y/b for all values of $\frac{S}{D}$ in Fig. 5.22. The velocities \bar{U}_c and \bar{U}_b correspond to the velocity at the centre line of wake ($Y=0$) and at the edge of the wake ($Y=b$) respectively. It may be observed that there is gradual recovery of velocity in the wake region with increase in $\frac{X}{D}$ for $\frac{S}{D} = 9$ & ∞ . But for $\frac{S}{D} = 5$ & 7 the change from $\frac{X}{D} = 3.0$ onwards is not systematic. These anomalous changes of velocity defect profiles at $\frac{X}{D} = 4$ & 5 for $\frac{S}{D} = 5$ & 7 may be attributed to the interference effect.

The velocity parameters $\frac{\bar{U}_c}{\bar{U}_0}$ and $\frac{\bar{U}_b}{\bar{U}_0}$ are plotted against $\frac{X}{D}$ in Fig. 5.24. It may be observed that $\frac{\bar{U}_b}{\bar{U}_0}$ decreases as $\frac{X}{D}$ increases whereas $\frac{\bar{U}_c}{\bar{U}_0}$ increases with $\frac{X}{D}$. Hence, $\frac{\bar{U}_b - \bar{U}_c}{\bar{U}_0}$ decreases with increase in $\frac{X}{D}$ as shown in Fig. 5.25. The non-dimensionalised length parameter $\frac{b}{D}$ variation with $\frac{X}{D}$ is also shown in Fig. 5.25. At $\frac{X}{D} = 2.0$ it appears that $\frac{b}{D}$ is independent of $\frac{S}{D}$.

The mean velocity in the region outside the wake zone non-dimensionalised as $\frac{\bar{U}_b - \bar{U}}{\bar{U}_b - \bar{U}_{se}}$ is plotted against $\frac{Y - \frac{S}{2}}{\frac{S}{2} - S}$



VELOCITY DEFECT IN THE WAKE ZONE NEAR THE WALL
FIG. 5-22



VELOCITY DEFECT OUTSIDE THE WAKE ZONE NEAR THE WALL
FIG. 5-23

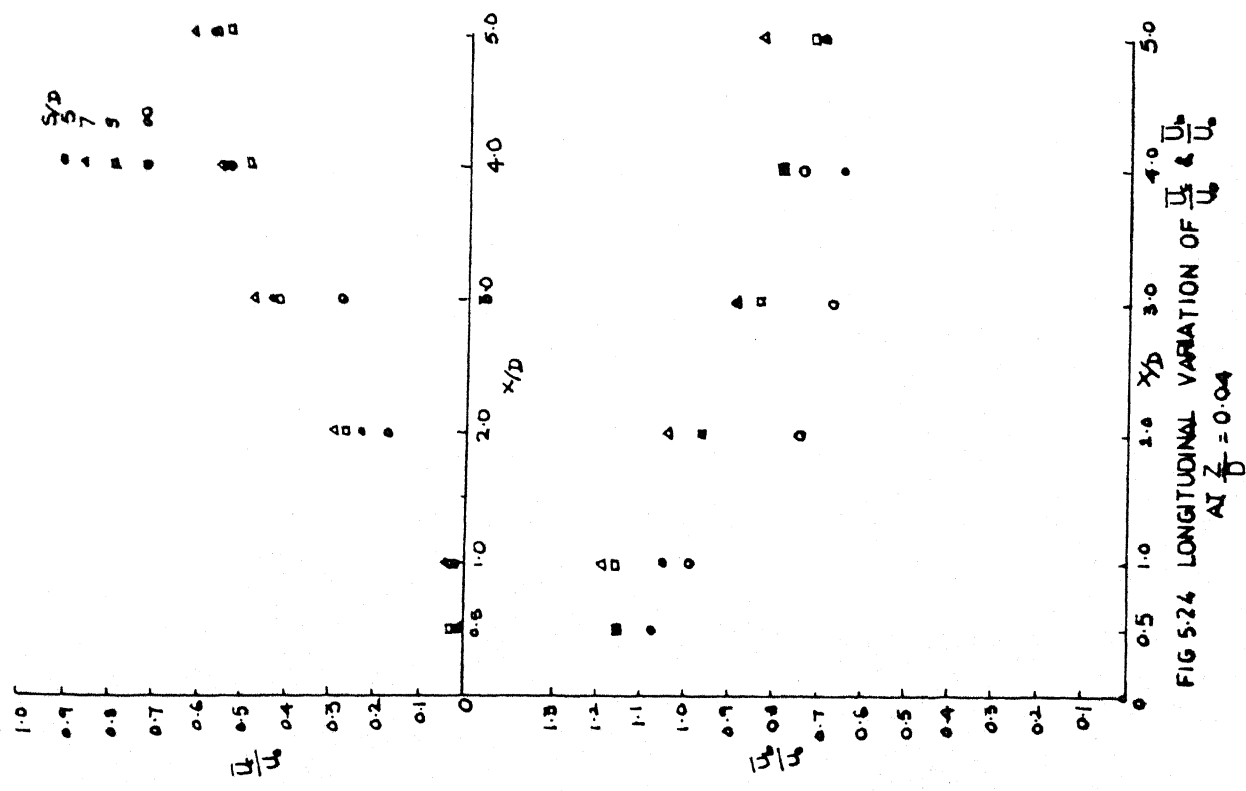


FIG 5.24 LONGITUDINAL VARIATION OF $\frac{U}{U_0}$ & $\frac{U_1}{U_0}$ AT $Z/D = 0.04$

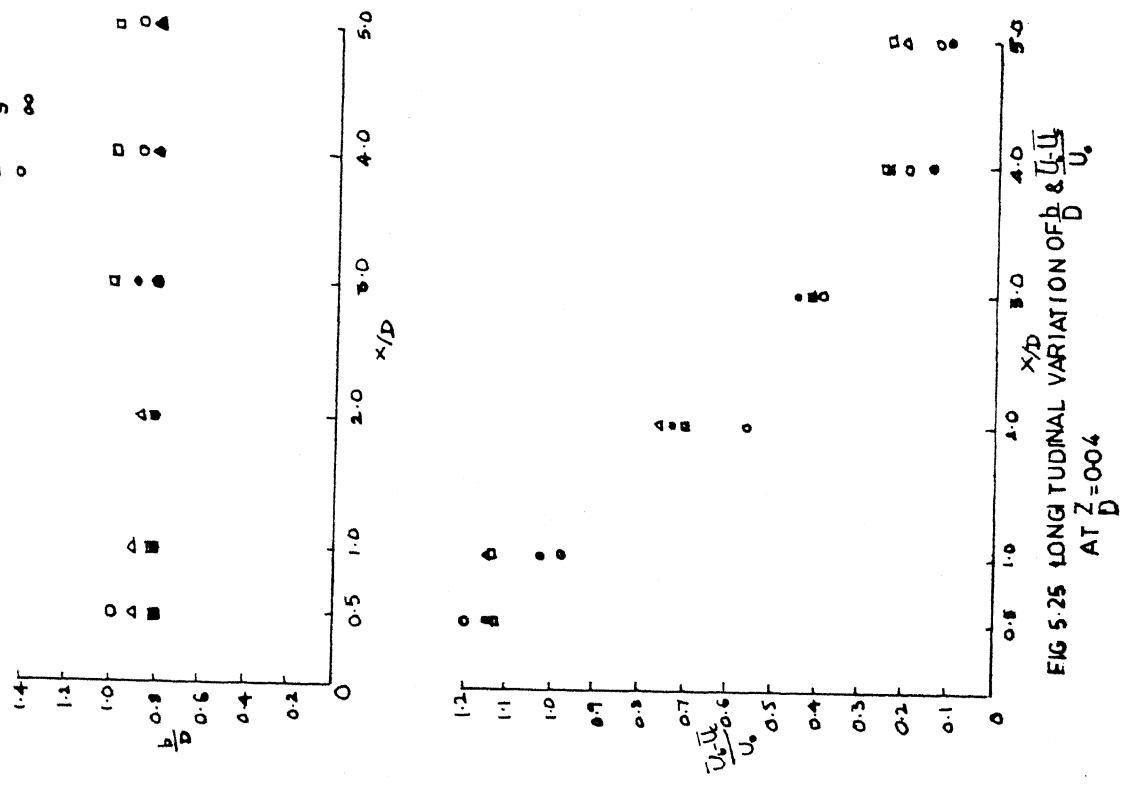


FIG 5.25 LONGITUDINAL VARIATION OF $\frac{U}{U_0}$ & $\frac{U_1}{U_0}$ AT $Z/D = 0.04$

for all values of $\frac{S}{D}$ as shown in Fig. 5.23. Here, $B = \frac{S}{2} - b$. The plot does not indicate any systematic variation.

5.8 INTERFERENCE EFFECT OF CYLINDERS :

When two cylinders are kept side by side at some lateral spacing, the flow distribution both inside and outside the wakes of cylinders gets modified due to mutual interference of cylinders. This modification is indicated by the variations of mean and RMS velocity distributions. In the present experimental study the following velocity changes are observed.

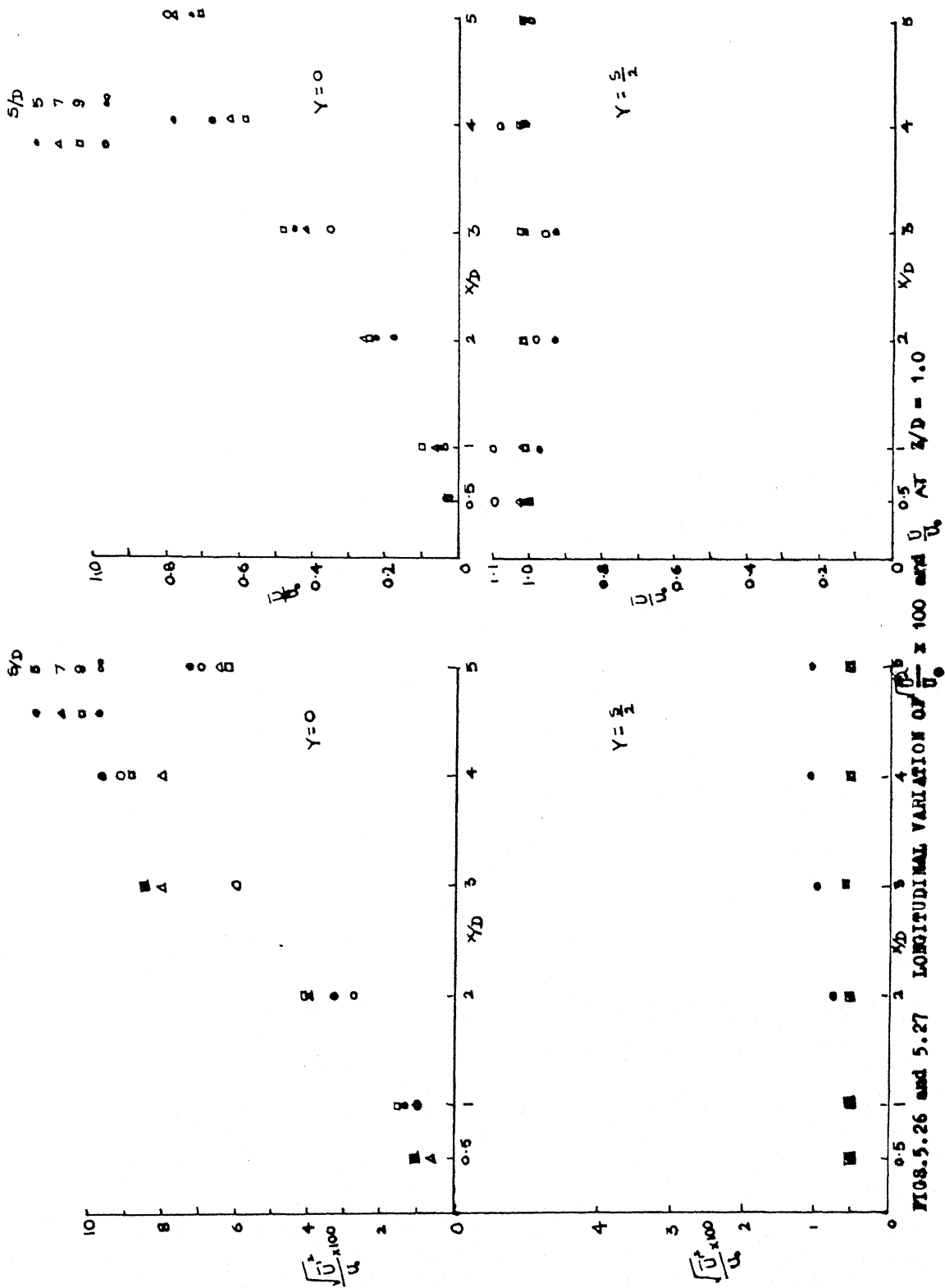
(1) Between the cylinders there is increase in the magnitude of free stream velocity in comparison to the approaching free stream velocity due to flow contraction. Consequently the increase in magnitude decreases with increase in lateral spacing as shown in Fig. 5.19.

(2) The vertical profile of mean velocity between the wakes of the cylinders becomes more uniform due to acceleration of flow as shown in Fig. 5.10. This can be observed as increase in value of power law exponent 'n' as shown in Fig. 5.17.

(3) The RMS velocity profiles at $Y = \frac{S}{2}$ (outside wakes) are similar to those in turbulent boundary layer flow. However, they are modified by the presence of two cylinders. The magnitude of maximum RMS velocity near the wall is found to increase with decrease of cylinder spacing as shown in Figs. 5.11 & 5.12.

(4) The RMS velocity in the wake region is also perceptibly affected by a neighbouring cylinder. The magnitude of RMS velocity in the region away from the wall along $Y = 0$ is found to have higher magnitude for $\frac{S}{D} = 5$ than for $\frac{S}{D} = 7$ and 9 as shown in Fig. 5.26.

In agreement with the literature cited in Chapter 2, it was noticed that the interference effect is almost negligible for $\frac{S}{D} = 5$. However, the present experimental investigation reveals an increase in RMS velocity components near the wall both in the wake zone and in the region between the wakes. This is significant for $\frac{S}{D} = 5$ but is also noticeable for $\frac{S}{D} = 7$ and 9. In the region between wakes, the hike in RMS velocity as well as its steep vertical gradient near the wall are indicative of the intense turbulent mixing in this zone. Obviously, turbulence energy is transferred more actively towards the boundary in this area than in the undisturbed flow region. Thus for bridge piers in alluvial soil the increased turbulence activity near the bed, due to mutual interference of the piers, can lead to higher local scour on the inner sides of piers. This accords with the observations made by Shah (1988) in his experiments on local scour around bridge pier.



CHAPTER 6

CONCLUSIONS AND SUGGESTIONS

CONCLUSIONS:

From the velocity measurements and graphical analysis attempted in this work, the following conclusions have been drawn about the flow characteristics downstream of circular cylinders placed in boundary layer flow in subcritical regime (pier Reynolds number $< 2 \times 10^5$).

1. Isolated Cylinder : The wake zone demarcated by the maxima of lateral variation of mean velocity is of fairly uniform width from a distance D downstream of cylinder. The vertical profile of mean velocity along the centre line of wake expands with increasing distance from the cylinder and approaches the mean velocity profile of the non-wake region. This indicates the predominance of wall effect over the wake effect sufficiently downstream of the cylinder. Along the centre lines of wakes, the RMS velocity variation over the vertical resembles mean velocity profiles of boundary layer flow. The high values of RMS velocity away from the wall, and their increase with increasing distance from the wall, indicate high turbulent activity in the wake region, particularly as it develops downstream.

2. Two Cylinders in lateral proximity :

a) **Wake region :** For lateral spacings used in the present work (5D, 7D and 9D), the distributions of the mean and RMS velocities in the X-Z plane passing through the centre line of a cylinder's wake closely resembles those of an isolated cylinder. However, the lateral variation of the mean and RMS velocities indicates increased turbulent activity towards the edge of the wakes. The wake zone is of fairly uniform width downstream of the cylinders, except for the spacing 9D when it shows an increase with downstream distance.

b) **Zone between wakes :** Along the centre line between wakes the near velocity in vertical profile is steeper than that of the undisturbed boundary layer flow; the maximum velocity is greater than the approaching free stream velocity. Hence, the flow is accelerating in this region. The RMS velocity distribution does not show much deviation from that in the undisturbed flow.

3. **Relation to local scour around bridge piers :** If the cylinders placed in turbulent boundary layer flow are compared to bridge piers in a river, the above results can throw some light on the scouring phenomena. Firstly, there exists in the wake flow high RMS velocities (turbulence energy) which should be capable of suspending much fine material as compared to the upstream flow. Secondly, when two piers are in lateral proximity,

not only can the wake flow suspend much material, but the high velocities at the edge of and between the wake regions can produce high shear stresses and erode bed material. This is the result of interaction of the flow affected by the two piers, and it vanishes for large spacings ($S > 9D$).

Suggestions for further study :

1. The present work is limited to velocity components in X-direction only. Measurements of velocity components in Y and Z direction simultaneously are necessary to give a three-dimensional picture of the flow field. Spatial correlation of the instantaneous velocity components and flow visualization techniques may be used to study the occurrence of eddies, horse-shoe vortices and vortex shedding.
2. Pressure tappings on the cylinder surface and wall boundary should be used to relate the observed changes in velocity distribution with pressure.
3. Measurements of flow characteristics in the boundary layer, separated flow zone and wake zone near the cylinder should be made to determine the drag and pressure coefficients, separation point, turbulence intensity and wall-effect in the flow immediately surrounding the cylinder.
4. Experiments should be conducted in turbulent water flow in a channel to make the results directly applicable to hydraulic problems, using rough or erodible beds.

REFERENCES

1. Baker, C.J., "Theoretical Approach to Predictions of Local Scour Around Bridge Piers", J. Hydraulic Research, Vol. 18, No.1, 1980, pp. 1 - 12.
2. Baker, C.J., "Laminar Horse-Shoe Vortex", J. Fluid Mech., Vol.95, 1979, pp. 347 - 367.
3. Basak, V., Basamisli, Y. and Ergun, O., "Maximum Equilibrium Scour Depth Around Linear-Axis Square Cross-Section pier Groups", Report No. 583, Ankara, 1975.
4. Bearman, P.W., and Wadcock, A.K., "The Interaction between a pair of circular cylinders normal to a stream", J. Fluid Mech., Vol. 61, 1973, pp. 499 - 511.
5. Biermann, D. and Hernstein, W.H., Jr., "The Interference between struts in various Arrangements", National Advisory Committee for Aerodynamics, Tech. Rep. 468, 1933.
6. Celik Ismail, "Analytical Modelling of Mean Flow Around Circular Cylinders - A Review", Advancements in Aerodynamics, Fluid Mechanics, and Hydraulics, ASCE, 1986, pp. 434 - 445.
7. Charles, G. Lomas., "Fundamentals of Hotwire Anemometry", Cambridge University Press.
8. El-Taher, R.M., "Flow Around Two parallel circular cylinders in a Linear Shear Flow", J. Wind Engg. and Industrial Aerodynamics, Vol.21, 1985, pp.251 - 272.
9. Elliot, K.R. and Baker, C.J., "Effect of Pier Spacing on Scour Around Bridge Piers", ASCE, JHD, Vol.111, No.7, 1985, pp. 1105 - 1109.

10. Gangadharaiiah, T., Muzzammil, Subramanya, K. and Kailash Gupta, "Vorticity Characteristics of Scouring Horse Shoe Vortex", Proc. Third International Workshop on Alluvial River Problems, 1989, pp. 19-26.
11. Hanen Kamp, W. and Hammer, W., "Transverse vibration Behaviour of cylinders in line", J. Wind Engg. and Industrial Aerodynamics, Vol.7, 1981, pp. 37 - 53.
12. Hinze, J.O., 1959, "Turbulence - An Introduction to it's mechanism and theory", McGraw Hill Book Company, New York.
13. Mori, E.T., "Experiments on Flow Around a pair of parallel circular cylinders", Proc. 9th Japan National Congress for Applied Mechanics, Tokyo, 1959, pp. 231 - 234.
14. Melville, B.W. and Raudkivi, A.J., "Flow characteristics in Local Scour at Bridge piers", J. Hydraulic Research, Vol.15, No.4, 1977, pp. 373 - 380.
15. Qadar, A., "The Vortex Scour Mechanism at Bridge Piers", Proc. Inst. Civil Engrs., 1981, pp. 739 - 757.
16. Roper, A.V., Schneider, R. and Shen, H.W., "Analytical Approach to Local Scour", Proc. IAHR, Vol.3, 1967, pp. 151 - 162.
17. Schlitching, "Boundary Layer Theory", Mc-Graw Hill Book Company, New York.
18. Shah, B.P., "Interference effects on Scour Depth Around Piers", M.Tech. thesis, IIT Kanpur, October, 1988.

19. Sharma, S.C., "Experimental Investigations of Vortex flow and it's Modifications Around Wall-Cylinder Junctions", Ph.D. thesis, Dept. of Aero. Engg., IIT Kanpur, July, 1988.
20. Shen, H.W., Schneider, M.R. and Karaki, S., "Local Scour Around Bridge Piers", ASCE, JHD, Vol. 95, HY 6, 1969, pp. 1919 - 1940.
21. Shiraishi, N., Matsumoto, M. and Shirato, H., "On Aerodynamic Instabilities of Tandem Structures", J. Wind Engg. and Industrial Aerodynamics, Vol.23, 1986, pp. 437 - 447.
22. Sikdar, S., "Study of Free Stream Turbulence in an Adverse Pressure Gradient", M.Tech. thesis, Dept. of Mech. Engg., IIT Kanpur, July, 1989.
23. Spivak, H.M., "Vortex Shedding Frequency and Flow pattern in the wake of Two parallel cylinders at varied spacings Normal to an Air Stream", J. of Aeronautical Sciences, Vol.13, 1946, pp. 289 - 297.
24. Zdrakovich, M.M. and Stanhope, D.J., "Flow pattern in Gap between two cylinders in Tandem", University of Salford, Internal Report, FM 5/72, 1972.
25. Zdrakovich, M.M., "Review of Flow Interference Between two cylinders in various Arrangements", J. Fluids Engg., Vol. 99, 1977, pp. 618 - 633.